Title

Chemical Evolution of Biomass Burning Aerosols across Wildfire Plumes in the Western U.S.: From Near-Source to Regional Scales.

Authors

Farley, Ryan

Zhou, Shan

Collier, Sonya

et al.

Publication Date

2025-04-11

DOI

10.1021/acsestair.5c00002

ACS ES&T Air

pubs.acs.org/estair

Article

Chemical Evolution of Biomass Burning Aerosols across Wildfire Plumes in the Western U.S.: From Near-Source to Regional Scales

Published as part of ACS ES&T Air special issue "Wildland Fires: Emissions, Chemistry, Contamination, Climate, and Human Health".

Ryan Farley, Shan Zhou, Sonya Collier, Wenqing Jiang, Timothy B. Onasch, John E. Shilling, Lawrence Kleinman, Arthur J. Sedlacek III, and Qi Zhang*

Cite This: ACS EST Air 2025, 2, 677−691

Read Online

ACCESS | Metrics & More | Article Recommendations | Supporting Information

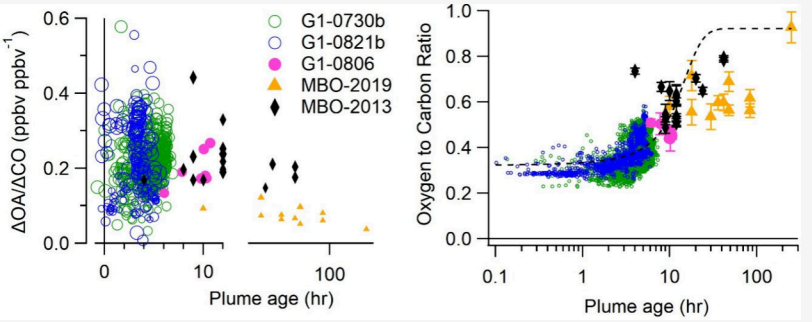

ABSTRACT: The atmospheric processing of biomass burning organic aerosol (BBOA) and its implications for tropospheric aerosol physicochemical properties remain uncertain. To address this gap, we investigate the chemical transformation of BBOA from wildfire events in the western U.S., using data from aerosol mass spectrometers aboard the DOE G-1 aircraft and at the Mt. Bachelor Observatory (∼2800 m a.s.l.) during the summers of 2013 and 2019. This study captures dynamic changes in submicron particulate matter (PM_1) concentrations and chemical profiles within wildfire plumes that span a broad range of atmospheric ages, from fresh emissions (<30 min) to plumes transported for several days. As plumes age, the oxidation state of organic aerosols (OA) increases, accompanied by the formation of secondary aerosol components such as phenolic secondary OA (SOA) species, carboxylic acids, and potassium sulfate. Early plume evolution is marked by the evaporation of semivolatile components and the formation of alcohol and peroxide functional groups, while extended aging produces more oxidized species, including carboxylic acids and carbonyl compounds. Normalized excess mixing ratios (NEMRs) of OA to CO demonstrate a complex interplay between evaporation, SOA formation, and oxidative loss. Using positive matrix factorization (PMF), we identify distinct BBOA types representing various stages of atmospheric processing and assess the contributions of primary BBOA and secondary BBOA formed through atmospheric reactions. These findings shed light on the intricate mechanisms governing the evolution of BBOA characteristics within wildfire plumes, providing critical insights to improve atmospheric modeling of BBOA and better assess the environmental and climatic impacts of wildfire emissions.

KEYWORDS: *biomass burning organic aerosol (BBOA), atmospheric aging, photochemical age, soot-particle aerosol mass spectrometer (SP-AMS), biomass burning observation project (BBOP), volatility basis set (VBS)*

1. INTRODUCTION

The release of aerosol into the atmosphere from wildfires carries adverse consequences on human health, global climate forcing, and regional air quality.[1−5] These impacts are particularly important for the western United States, a region that has experienced a recent surge in the intensity and frequency of wildfire events. These events have given rise to recurrent and widespread severe air pollution episodes, notably during the summer and fall months.[6−9]

Wildfires, like biomass burning (BB) in general, emit a complex mixture of primary organic aerosol (POA), inorganic species such as black carbon (BC), and volatile organic compounds (VOCs) which can react in the atmosphere to form secondary organic aerosol (SOA).[10] Within BB plumes,

Received: January 1, 2025
Revised: March 14, 2025
Accepted: March 14, 2025
Published: March 28, 2025

organic aerosol (OA) constitutes a dominant fraction of submicron aerosol (PM_1), followed by BC and particulate chloride and nitrate.[11] As they disperse through the atmosphere, BB plumes undergo a multitude of physical and chemical processes that lead to dynamic variations in both aerosol loading and composition, ultimately impacting their radiative forcing contributions through both direct and indirect effects. For instance, oxidation reactions involving VOCs and ·OH, O_3, or $\cdot NO_3$ radicals in the gas phase can yield lower volatility species, which have the potential to condense and form SOA.[12−14] Additionally, heterogeneous and aqueous-phase reactions within BB plumes could contribute to both accretion reactions, leading to the formation of SOA, and fragmentation reactions, resulting in the net loss of OA mass.[15−19] The chemical and physical transformations occurring within wildfire plumes have significant impacts on aerosol characteristics pertinent to climate dynamics. These changes include both the formation of brown carbon (BrC) species and photobleaching processes.[20,21] Moreover, the production of oxygenated species can significantly increase the overall hygroscopicity of aerosols within wildfire plumes, even though primary BBOA and BC are inherently hydrophobic.[22]

In addition to chemical transformations, material within BB plumes is transferred between the gas and aerosol phases as the system approaches an equilibrium dependent on the vapor pressure of the species, OA concentration, and particle-phase state.[23] When dense BB plumes mix with clean background air, a greater proportion of semivolatile material partitions from the particle phase to the gas phase due to dilution-induced evaporation, leading to changes in aerosol chemical properties within wildfire plumes.[24] For instance, at the plume edge, where dilution effects are more pronounced compared to the central core, aerosols exhibit reduced signal intensity from anhydrous sugars (indicative of primary BBOA), alongside an enhanced oxygen-to-carbon ratio (O:C).[24,25] However, these variations may also arise from enhanced photochemistry near the plume edges due to increased light transmission, resulting in a higher ·OH concentration.[26]

Normalizing OA to excess CO (ΔOA/ΔCO) to account for dilution offers a valuable approach to study the transformations of OA in BB plumes throughout atmospheric processes. An increase of ΔOA/ΔCO with plume age suggests the formation of SOA, while a decrease indicates the loss of organic matter due to evaporation, fragmentation reactions, and deposition.[27,28] Laboratory studies have found an increase in ΔOA/ΔCO when BB smoke undergoes oxidative processing;[29] however, field studies have shown varying results, with some measuring an increase,[30] some showing a decrease,[31−33] and others seeing no change in ΔOA/ΔCO with aging.[34−36]

One hypothesis to account for the negligible change of ΔOA/ΔCO seen during field studies is that the formation of SOA is offset by dilution-driven evaporation of semivolatile POA.[31,34,36] However, this scenario still results in changes in the chemical composition of the OA, as semivolatile and reduced species are replaced with highly oxygenated, lower volatility compounds.[20,36,37] Few studies have explored dilution-induced changes in BBOA characteristics, with most focusing on the initial few hours of physical aging.[24,29,37−39]

Aircraft-based measurements play a crucial role in investigating the evolution of wildfire plumes, typically spanning from near-field to hours of physical aging.[19,39−41] A study conducted using aircraft in West Africa sampled agricultural burning plumes after 0.5 to 12 h of aging, revealing significant changes in OA composition and suggesting rapid atmospheric processing.[35] While aged wildfire plumes up to several days old have also been studied from aircraft platforms,[21,42] remote mountaintop sites offer the advantage of sampling transported plumes over a broader range of processing times with minimal interference from local emissions. This includes measurements of BB plumes that have undergone substantial atmospheric processing for as long as 2 weeks.[27,33,36,43−45] By combining aircraft and mountaintop measurements, we gain a more comprehensive understanding of how wildfire plumes evolve over time, encompassing both the immediate effects and the long-term changes caused by atmospheric processing.[43]

Both aircraft- and ground-based studies of wildfire events commonly employ aerosol mass spectrometers (AMS) to track the composition, sources, and transformations of aerosols originating from wildfires. The integration of positive matrix factorization (PMF) with AMS measurements has successfully resolved BBOA factors across diverse atmospheric environments.[15,33,36,46−48] Furthermore, this approach has also led to the identification of multiple BBOA factors that represent different stages of atmospheric processing of wildfire plumes, providing valuable insights into the evolutionary path of BBOA in the atmosphere.[36]

In this study, we analyze measurements of wildfire plumes from the DOE Gulfstream-1 (G1) aircraft and at the Mt. Bachelor Observatory (MBO; ∼2800 m a.s.l.) as part of the 2013 Biomass Burning Observation Project (BBOP) sponsored by the U.S. DOE.[49] The G1 aircraft was equipped with a suite of particle and gas-phase instrumentation, including a high-resolution soot particle time-of-flight aerosol mass spectrometer (hereafter SP-AMS) sampling at 1 Hz for PM_1 composition quantification. From July to September 2013, the G1 aircraft was based out of Pasco, Washington and sampled wildfire plumes across Washington, Oregon, and Idaho, with a focus on fresh plumes that had undergone processing for less than a few hours.[36,39,43] The MBO is a mountaintop atmospheric monitoring site that has been used extensively to characterize transported plumes originating from local, regional, and intercontinental wildfire events.[36,50−52] A high-resolution time-of-flight AMS (HR-ToF-AMS) was deployed at MBO during BBOP, capturing data from wildfire plumes aged between 6 and 48 h. Additionally, an SP-AMS was deployed at MBO during the summer of 2019 where extensively aged wildfire plumes (some up to 2 weeks) were observed.[33] By combining these data, we comprehensively characterize the evolution of wildfire plumes, ranging from those with less than 30 min of processing time to those subjected to multiple days of physical transport. Our primary focus lies in understanding the changes in BBOA composition through unraveling the associated chemical processes and examining the formation of SOA via PMF analysis. Additionally, we explored the emergence of specific secondary compounds during the transport process.

2. EXPERIMENTAL AND DATA ANALYSIS METHODS

2.1. Measurements of Wildfire Plumes from Aerial and Mountaintop Platforms. We focus on measurements obtained during three G1 flights in 2013 and at the MBO ground site during both 2013 and 2019. Details regarding the AMS operations aboard the G1 aircraft and at MBO are described in previous publications,[27,33,36,39,53,54] and additional

https://doi.org/10.1021/acsestair.5c00002
ACS EST Air 2025, 2, 677−691

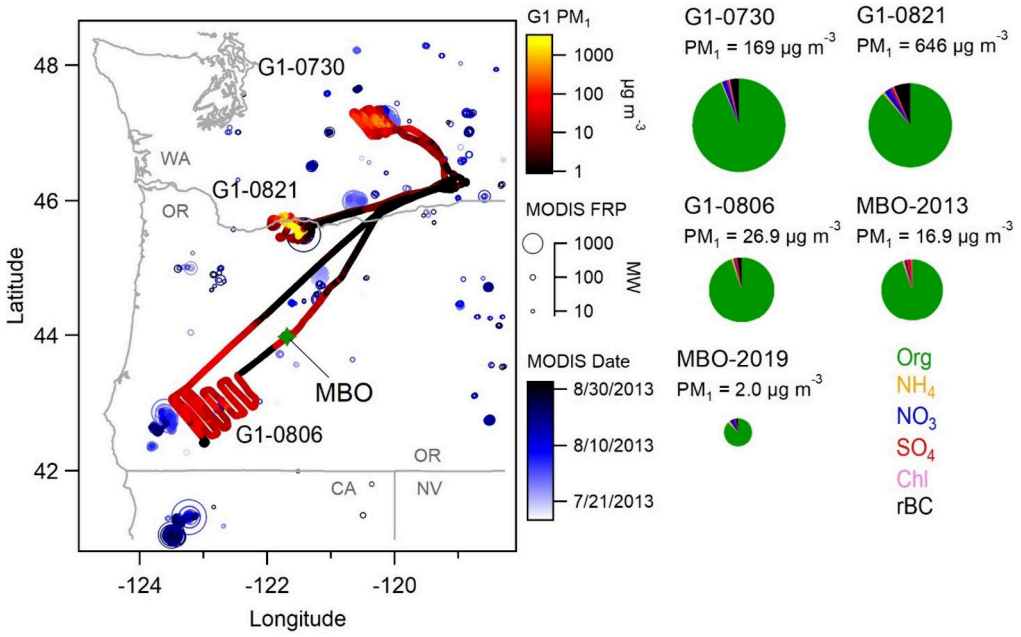

Figure 1. Map of the U.S. Pacific Northwest region featuring the flight paths of the G1 research flights used in this analysis, color-coded based on PM_1 concentration. Open circles indicate thermal anomalies detected by the MODIS satellite colored by date and sized by fire radiative power (FRP). Pie charts represent average PM_1 composition measured by SP-AMS, with pie chart size corresponding to the average $\log_{10}(PM_1)$.

Table 1. Summary of Wildfire Characteristics Observed During G-1 Research Flights

fire name	data set	MCE[a]	primary fuel	acres burned	dates burned
Colockum Tarps fire	G1-0730	0.92 ± 0.005	shrubland (sagebrush)	80,000	7/17/13–8/14/13
Government Flats fire	G1-0821	0.92 ± 0.006	conifer forest (ponderosa pine, grand fir)	11,400	8/17/13–8/26/13
Whisky Creek complex	G1-0806, MBO-2013	N/A	mixed conifer forest (Douglas fir, ponderosa pine, sugar pine, California black oak)	14,000	8/10/13–9/6/2013
Salmon River complex	G1-0806, MBO-2013	N/A	mixed conifer forest (Douglas fir, ponderosa pine, sugar pine, California black oak)	14,700	7/31/2013–8/31/2013
Douglas complex	G1-0806, MBO-2013	N/A	mixed conifer forest (Douglas fir, ponderosa pine, sugar pine, California black oak)	45,000	7/18/2013–10/24/2013

[a]Kleinman et al., 2020.[39]

information on the BBOP campaign can be found in Section S1.1. Specifically, two flights (G1-0730b and G1-0821b) were chosen as they sampled significant, well-defined wildfire plumes in a pseudo-Lagrangian pattern, including transects upwind, directly over, and up to approximately 50 km downwind of the emissions sources (Figure 1). The flight on the afternoon of July 30, 2013 (G1-0730b) sampled emissions from the Colockum Tarps fire in central Washington, while the flight on August 21, 2013 (G1-0821b) sampled emissions from the Government Flats fire in northern Oregon (Figure 1). A third research flight (G1-0806) was conducted on August 6, 2013, and sampled locally and regionally transported plumes from the Douglas and Whisky complexes in southern Oregon and the Salmon complex in northern California (Figure 1). A summary of the characteristics of the different wildfire plumes is presented in Table 1. The G1-0806 flight was strategically coordinated with measurements at MBO and included a direct fly-by (Figure 1). A comparison of pollutant measurements between these two platforms is summarized in Table S1 of the Supporting Information.

The HR-ToF-AMS was deployed at MBO from July 25 to August 25, 2013, and the SP-AMS was deployed from August 1 to September 10, 2019. Wildfire smoke events at MBO were defined as periods characterized with (1) elevated levels of OA, CO, and CO_2 above the background and (2) high correlations ($r^2 > 0.6$) between CO and PM_1.[27,33,55]

2.2. Positive Matrix Factorization (PMF) Analysis of SP-AMS Data. We expect that all OA sampled during the G1 smoke transects can be attributed to a set of BBOA factors that represent either varying stages of atmospheric processing or distinct emission profiles due to different fuel types and combustion conditions. Due to the high aerosol loadings within the wildfire plumes relative to the regional background, any contribution from biogenic SOA is assumed to be negligible. To identify these distinct BBOA types, source apportionment analysis was conducted by applying positive matrix factorization[56,57] to the AMS data separately for each research flight using the ME-2 algorithm within SoFi Pro v9.4 based in Igor 9.[58] For each data set, one factor was constrained to the highly oxidized BBOA-3 factor identified by Zhou et al.[36] using the *a*-value approach, while the other factors were allowed to vary freely. A three-factor solution was chosen for G1-0821b and G1-0806, while a four-factor solution was chosen for G1-0730b. Subsequently, each PMF factor was

https://doi.org/10.1021/acsestair.5c00002
ACS EST Air 2025, 2, 677–691

categorized as fresh BBOA (F-BBOA), aged BBOA (A-BBOA), and highly aged BBOA (HA-BBOA) based on their oxidation state and position within the f_{44}/f_{60} space. For the G1-0730b flight, a second fresh BBOA factor is necessary to explain the variation in the aerosol composition, likely due to variable fuels with different emission profiles. Further details on the PMF analysis and results are included in Section S1.2.

The unconstrained PMF solutions for the MBO mountaintop site during BBOP and 2019, described in Zhou et al.[36] and Farley et al.,[33] respectively, are used in this study as well. Specifically, during BBOP, three distinct BBOA factors were resolved at the MBO, including a fresh BBOA (BBOA-1), a moderately aged BBOA (BBOA-2), and a highly aged BBOA (BBOA-3). During the 2019 measurements, there was significantly less influence from fresh wildfire smoke, and only a single BBOA factor was resolved with properties intermediate of the BBOA-2 and BBOA-3 factors.

2.3. Calculation of Normalized Excess Mixing Ratios (NEMRs). The NEMR of different species was calculated to account for plume dilution. For the G1-0730b and G1-0821b flights, this procedure was carried out on a point-by-point basis to account for rapid variations in plume composition sampled by the aircraft using the following equation:

$$\left(\frac{\Delta X}{\Delta CO}\right)_i = \frac{X_i - X_{bckgd}}{CO_i - CO_{bckgd}} \quad (1)$$

where X_i and CO_i represent the concentrations of species X and CO at a given time point *i*. X_{bckgd} and CO_{bckgd} denote the background concentrations of X and CO, which were defined as the tenth percentile of the respective species measured at MBO during BBOP, as this site is generally representative of the background conditions of the western U.S.[53,59] Specifically, the values of CO_{bckgd} and OA_{bckgd} were determined to be 0.08 ppm and 2.35 μg sm^{-3}, respectively. ΔOA/ΔCO was calculated in units of ppbv ppbv^{-1} using an average molecular weight of 250 g mol^{-1} for OA.

Due to the lower concentrations measured at MBO and during the G1-0806 research flight, NEMRs were determined for each smoke event based on the orthogonal distance regression of the species X and CO to better account for variations in background CO and PM_1.[27,33,36]

2.4. Calculation of Photochemical Age and Physical Transport Time of BB Plumes. The aerosol photochemical age was calculated based on the change in NO_x concentration relative to CO. NO_x and CO are both primary species emitted during combustion; however, NO_x reacts quickly with ·OH, while CO is relatively inert in the atmosphere. Thus, photochemical age can be calculated using the following equation:

$$t = \frac{1}{[\cdot OH]k_{NO2+OH}}\left[\ln\left(\frac{[NO_x]}{[CO]}\right)_{t=0} - \ln\left(\frac{[NO_x]}{[CO]}\right)\right] \quad (2)$$

where t is time in seconds, [·OH] is the ambient concentration of ·OH radical (assumed to be 1×10^7 cm^{-3}), and k_{NO2+OH} = 1.07×10^{-11} molecules cm^{-3} s^{-1}.[60] The ·OH radical concentration was selected to provide moderate agreement between the photochemical age and the physical transport (Figure S1). Additionally, this value agrees with other in situ · OH measurements within wildfire plumes.[26,30] $([NO_x]/[CO])_{t=0}$ is the emission ratio of NO_x (ER_{NOx}) at the point of emission. The ER_{NOx} for G1-0730b and G1-0821b, defined as the highest 10 s average NO_x/CO ratio observed during the flight, were 9.52×10^{-3} and 17.8×10^{-3}, respectively, and show reasonable agreement with previous literature measurements of $9.2(\pm0.6) \times 10^{-3}$, $8.0(\pm0.3) \times 10^{-3}$, and $9.1(\pm7) \times 10^{-3}$.[10,32,61] The higher ER_{NOx} seen during G1-0821 may stem from differences in fuel type or combustion efficiency during this wildfire.[62] Indeed, Andreae reports higher values for temperate forests ($24(\pm17) \times 10^{-3}$) than boreal forests ($9.1(\pm7) \times 10^{-3}$), highlighting the importance of fuel type. It is also noteworthy that as ER_{NOx} was defined after a brief processing period, the photochemical age may represent a lower limit and does not account for the plume rise time. Further details on the calculation of photochemical age are provided in Section S1.3.

For the G1-0806 and MBO measurements, all sampled BBOA had undergone some degree of processing; therefore, the ER_{NOx} was set to 9.2×10^{-3} based on Simpson et al.,[61] due to the similarity in fuel types. For each smoke event identified during G1-0806 and at MBO, a single NO_x/CO value was calculated following the methodology used for calculating the NEMR discussed in section 2.3. Specifically, the orthogonal distance regression with the *y*-intercept allowed to vary was calculated for each event. No calculations of photochemical age were conducted for smoke events with an $r^2 < 0.5$ between NO_x and CO. This included one of the 10 events during the G1-0806 flight and 13 of the 18 events sampled at MBO during BBOP. The low correlations likely resulted from either the mixing of different sources or the complete depletion of NO_x from the airmass.

The physical transport times for the G1-0730b and G1-0821b plumes were calculated by dividing the distance between the aircraft and the emission source by the windspeed measured by the aircraft at the time of sampling, and a comparison is shown in Figure S1a. The location of the plume emission was determined by identifying thermal anomalies detected by MODIS aboard the Aqua and Terra satellites. For the smoke events captured during G1-0806 and at MBO, the physical transport time was estimated through a comparison of back trajectories obtained by using the HYSPLIT model and the MODIS thermal anomalies. Further details regarding this approach can be found in the works by Collier et al.[27] and Farley et al.[33] Unless otherwise specified, we use the photochemical age for G1 research flights and the physical age for the plumes sampled at MBO. When taken together, we use the more general term plume age.

2.5. Quantification of Aerosol Volatility. The volatility of aerosol particles was characterized at the MBO site during both the 2013 and 2019 studies using a digitally controlled thermodenuder (TD) system positioned upstream of the AMS.[33,36] The TD operation was automated via a custom program that cycled through 12 different temperatures ranging from 30 to 280 °C, with 10 min intervals. An automatic three-way ball valve facilitated the transition of the aerosol flow between the TD and the bypass sampling modes every 5 min. During the bypass mode, the temperature inside the TD was brought to thermal equilibrium with the next preset temperature before switching back to the TD mode. PMF analysis was conducted on the data set comprising mass spectra acquired from both the TD and the bypass modes, thus allowing for the determination of the thermal profiles of individual OA factors. The thermograms were converted to volatility basis sets (VBS)[23] using the kinetic evaporation model described in the

https://doi.org/10.1021/acsestair.5c00002
ACS EST Air 2025, 2, 677−691

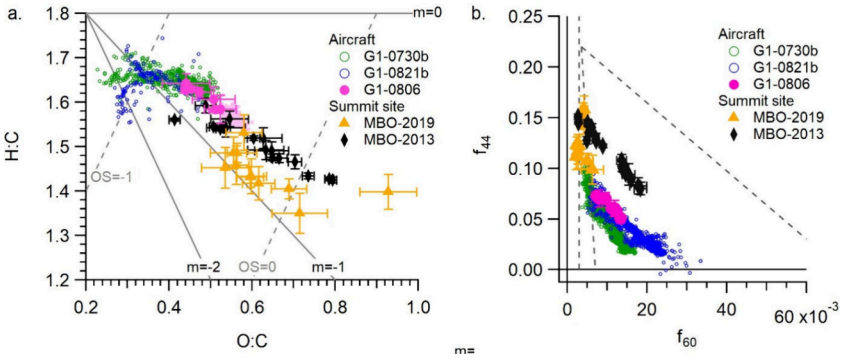

Figure 2. (a) Van Krevelen diagram plotting bulk H:C and O:C and (b) f_{44}/f_{60} triangle plot for BBOA in the wildfire plumes observed in this study. Error bars indicate the standard deviation during each plume event.

work by Cappa.[63] Details of this calculation are provided in Section S1.4.

3. RESULTS AND DISCUSSION

3.1. Overview of Wildfire Plumes of Varying Transport Ages. The measurements analyzed here encompass wildfire emissions that have undergone between 30 min and 2 weeks of atmospheric processing. While the plumes gradually mix with background air during transport and become diluted, it is important to note that the G1 flights and the MBO site were located within the free troposphere, where the background air is expected to be clean.[53] Therefore, the presence of PM from sources other than BB is expected to be negligible compared to the smoke particles in the plumes studied here.

Both the G1-0821b and G1-0730b flights employed a pseudo-Lagrangian sampling approach and captured fresh plumes typically within 30 min postemission during their closest transects (Figure 1). These transects exhibited the highest PM_1 and CO concentrations, with maximums of 9753 μg sm^{-3} (at standard temperature and pressure of 273.15 K, 1 atm) and 16 ppmv, respectively, for G1-0821b and 2803 μg sm^{-3} and 5.1 ppmv, respectively, for G1-0730b. As the distance from the source increased, the plume gradually mixed with cleaner background air and became increasingly dilute. The substantially lower concentrations observed near the outer edges of each transect indicate well-defined plume structures and low background PM_1 concentrations.

The G1-0806 research flight sampled wildfire emissions that were more dilute compared to the other two G1 flights yet still exhibiting PM_1 substantially elevated above background concentrations, peaking at 365 μg sm^{-3}. Considerably more spatial homogeneity was seen across individual transects during this flight, suggesting that the plume had mixed more extensively with the regional background air (Figure 1). Throughout all three research flights, OA contributed the dominant fraction of PM_1, accounting for >89% of total mass. Following this was refractory BC (2−6%), while chloride, sulfate, nitrate, and ammonium each accounted for ≤2% of total PM_1 (Figure 1).

The BB plumes characterized at the Mt. Bachelor summit site had undergone significantly longer transport durations. During the 2013 campaign, a series of wildfires occurred about 200−350 km upwind of MBO in southern Oregon and northern California, and the results from this study have been documented in previous publications.[27,36,43,53,64] In the present study, we utilize 18 BB smoke events with clearly identified emission sources and estimated physical transport times ranging from 4 to 42 h.[27] These smoke events were identified based on strong correlations ($r^2 > 0.85$) between CO and CO_2. Additionally, we incorporate 11 smoke events sampled at MBO in 2019, with physical transport time ranging from 10 to 250 h.[33] Due to the lower concentrations, slightly less stringent criteria were used, with smoke events defined as periods with a correlation between CO and PM_1 of $r^2 > 0.6$ and a CO concentration greater than 110 ppb. As shown in Figure 1, despite substantial variations in aerosol loadings, wildfire smoke events observed at MBO exhibit aerosol compositions similar to those observed during the G1 flights.

Back-trajectory analysis indicates that the BB-influenced airmass sampled during the G1-0806 flight was directly transported to the MBO, allowing for the analysis of wildfire plumes originating from the same emission source but experiencing significantly longer transport times, thereby eliminating the effect of variations in fuel type and combustion efficiency. Furthermore, the excellent agreements between the average pollutant concentrations and aerosol properties observed aboard the G1 and at MBO during a direct fly-by (Table S1) instill confidence in merging the data sets from both platforms for subsequent analyses on BBOA evolution. However, as the fires sampled by G1-0730b and G1-0821b were in different geographic regions, there may be systematic differences in the fire characteristics.

3.2. Chemical Evolution of Aerosols in Wildfire Plumes during Atmospheric Aging. *3.2.1. Evolution of Bulk BBOA Properties and Oxidation State.* Despite variations in sampling locations, the trends in aerosol evolution display similar patterns across different plumes. Given the predominance of BBOA in the plumes analyzed in this study, we explore the atmospheric processing of BBOA using the Van Krevelen diagram, where bulk H/C is plotted against O/C, and the slope of the relationship provides insights into the dominant chemical reaction types (Figure 2a).[65] A slope of 0, −1, and −2 corresponds to the addition of alcohol/peroxide functional groups, carboxylic acid, and carbonyl groups, respectively. Previous ambient measurements in locations dominated by biogenic or anthropogenic emissions have typically shown slopes near −1,[65,66] while measurements of ambient BBOA have revealed slopes closer to zero.[48,67] However, experiments involving the aging of BB smoke in an oxidative flow reactor have indicated that ·OH oxidation of BBOA from most biomass fuels yields a slope close to −0.5, except for ponderosa pine smoke, which exhibits a slope of nearly zero.[28]

https://doi.org/10.1021/acsestair.5c00002
ACS EST Air 2025, 2, 677−691

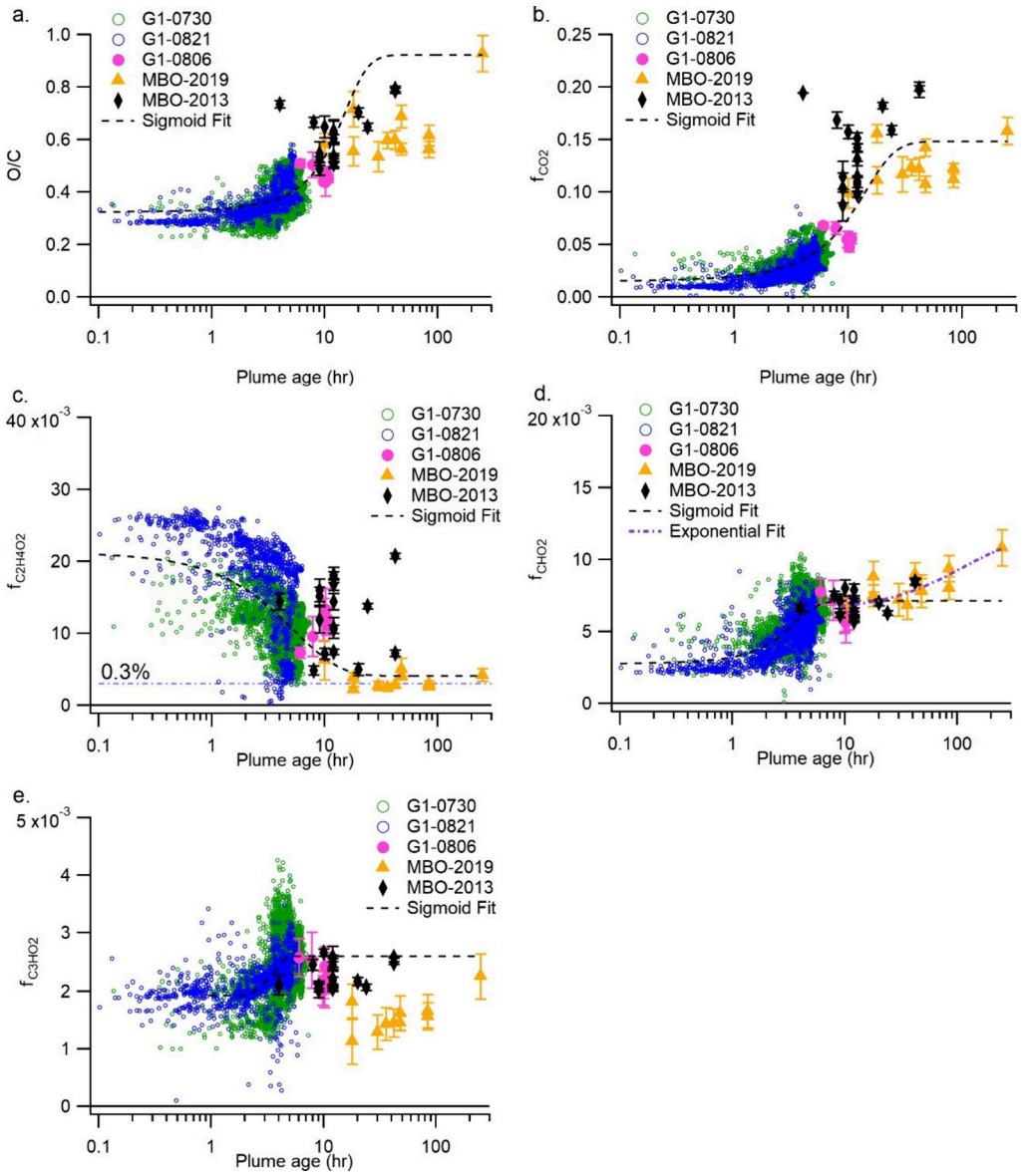

Figure 3. Change in (a) O/C, (b) f_{CO2}, (c) f_{C2H4O2}, (d) f_{CHO2}, and (e) f_{C3HO2} with plume age. Plume age is defined as the photochemical age for the G1 measurements and as the physical age for the MBO measurements. A sigmoid function is applied to fit all of the data points. In (d), an exponential fit for f_{CHO2} data points at more than 10 h is also included.

As shown in Figure 2a, the plume transects sampled during the G1-0821b and G1-0730b flights demonstrate slopes of 0.05 and −0.15, respectively, suggesting the formation of alcohol or peroxide functional groups during the aging of freshly emitted wildfire plumes. This near-zero slope is especially apparent at O/C < 0.5, i.e., during the initial 2 to 3 h of photochemical aging. Beyond that, the slopes gradually decrease, and the G1-0806 and MBO-2013 plume events show negative slopes of −0.58 and −0.54, respectively. The trend observed during the MBO-2019 plume events generally aligns with those of G1-0806 and MBO-2013, although the correlation between O/C and H/C is weaker (r^2 = 0.32). This weaker correlation could be attributed to the relatively low BBOA concentrations and longer atmospheric transport times within the MBO-2019 plumes, resulting in a stronger influence from background aerosols, such as biogenic SOA.[33] Taken together, these results indicate that while near-field processing primarily involves the formation of alcohol or peroxide moieties, the formation of carboxylic acids or carbonyl functional groups becomes increasingly prominent with extended aging. This observation aligns with laboratory studies investigating the formation and photochemical transformation of SOA derived from the oxidation of phenols—a major class of VOCs emitted during biomass burning.[17,68−71]

The evolution of the chemical properties of BBOA can also be visualized through the f_{44}/f_{60} triangle plot originally introduced by Cubison et al. (Figure 2b).[31] f_{60}, the fraction of organic mass at m/z 60 (mostly $C_2H_4O_2^+$), is a tracer for anhydrous sugars including levoglucosan, while the fraction of mass at m/z 44 (f_{44}; mostly CO_2^+) is a marker for oxidized OA, including carboxylic acids. Upon oxidation, f_{60} decreases while f_{44} increases in the AMS spectra of BBOA. All of the wildfire plumes examined in this study show a similar trend upon oxidative aging, as indicated by the parallel slopes transitioning from the bottom right to the top left of the f_{44}/f_{60} plot (Figure 2b). For this analysis we utilize the f_{44} and f_{60}

https://doi.org/10.1021/acsestair.5c00002
ACS EST Air 2025, 2, 677−691

variables for a direct comparison with previous studies. However, in the following section, we use the fraction of mass of the CO_2^+ ion (f_{CO2}) and $C_2H_4O_2^+$ ion (f_{C2H4O2}) to eliminate interference from ions with the same nominal mass.

The increase in bulk O/C and f_{CO2} and the decrease in f_{C2H4O2} all exhibit sigmoid relationships with plume age, with little change in these parameters for plumes younger than 1 h (Figure 3). However, plumes aged between 1 and 4 h experience a sharp decrease in f_{C2H4O2}, accompanied by only a minimal corresponding increase in f_{CO2}. Conversely, the most pronounced upward trend of f_{CO2} is observed between 5 and 20 h of aging. This pattern is consistent with the loss of semivolatile materials, such as levoglucosan, prior to the formation of highly oxidized SOA species such as carboxylic acids. Additionally, the notable rise in the O/C ratio within plumes aged between 3 and 20 h (Figure 3a) suggests that this duration of aging induces the most significant and rapid changes in BBOA composition. This aligns with the findings of Sedlacek et al.,[19] who studied plume aging through changes in the black carbon coating thickness. Their study observed an initial increase in coating thickness, followed by a decrease after 0.5 to 1 day of atmospheric processing. This time scale is similar to the present work, where markers for the formation of SOA show significant increases within the first 24 h. However, we continue to observe increases in these signatures as atmospheric aging continues.

3.2.2. Evolution of Secondary BBOA Species. Phenolic compounds, such as phenol (C_6H_6O), guaiacol ($C_7H_8O_2$), catechol ($C_6H_6O_2$), and guaiacyl acetone ($C_{10}H_{12}O_3$), are emitted in large quantities from BB[72,73] and can react in the gas or aqueous phase to form SOA compounds, including hydroxylated phenols, nitrophenolic compounds, and oligomers.[17,68−71] Phenolic SOA is an important component of secondary BBOA and has an outsized impact on aerosol absorption and toxicity.[20,74] It is also thought that nitrophenol compounds are an important component of tarballs, which are light absorbing aerosols commonly found within wildfire plumes.[54,75] Laboratory studies have identified a number of HR-AMS fragments that are indicative of phenol SOA.[17,68,76] Furthermore, studies have shown that during prolonged photochemical aging, the composition of phenolic SOA undergoes a transition from being dominated by large multifunctional compounds to smaller, highly oxygenated species, such as carboxylates.[18,69,77]

The CHO_2^+ fragment serves as a mass spectral tracer ion for carboxylates.[17] Figure 3d shows that the fraction of mass at CHO_2^+ (f_{CHO2}) evidently increases as a function of the plume age. Interestingly, this increase occurs earlier and at a faster rate than the increase in f_{CO2}, with an inflection point of the sigmoid relationship at 2.7 h, in contrast to 8.5 h for f_{CO2} (Figure 3d). Furthermore, f_{CHO2} exhibits a continuing upward trend even in the most aged plume measured (Figure 3d). The $C_3HO_2^+$ fragment, prominent in the AMS spectra of phenolic SOA and likely derived from unsaturated carbonyls,[76,78] shows a less well-defined trend; however, a good correlation with CHO_2^+ is seen in plumes less than 12 h old (r^2 = 0.92−0.95). These findings further emphasize the increased presence of carboxylic acids or carbonyl functional groups in more aged BBOA.

Although the absolute concentration of nitrogen-containing organics in smoke plumes is generally low, they are an important component of brown carbon (BrC) and can have an outsized role on aerosol absorption.[20] The fraction of the nitrate signal attributed to organonitrates (f_{pRONO_2}) was estimated using the ratio of NO^+ and NO_2^+ and is described in Section S1.1. f_{pRONO2} shows a decrease with increasing nitrate concentration (Figure 4), a trend similar to findings

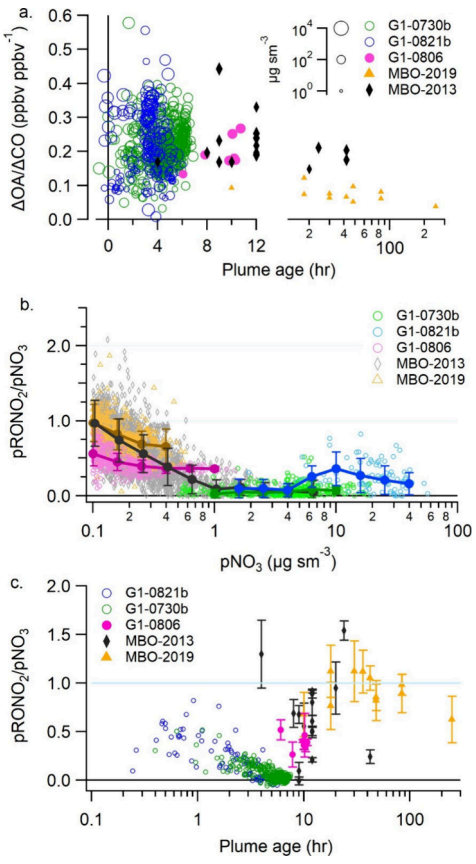

Figure 4. (a) Change in the NEMR of OA (ΔOA/ΔCO) with plume age in wildfire plumes. (b) Variation in the fractional abundance of organonitrate relative to total particulate nitrate (f_{pRONO_2}) as a function of total particulate nitrate concentration. Solid lines indicate the binned average, and errors bars indicate one standard deviation. (c) Changes of f_{pRONO_2} as a function of plume age. In (a), symbols are sized by the log-transformed organic aerosol loading; the *x*-axis transitions to log scale at 12 h.

reported in other studies.[79,80] At the MBO, nearly all of the nitrate signal was associated with inorganic nitrate during BB periods. However, $pRONO_2$ was found to dominate the total nitrate signal during clean periods, contributing ∼5% of the total OA and likely formed from the reaction of biogenic monoterpenes.[53] In contrast, both G1-0730b and G1-0821b exhibit an inverse relationship, with periods of higher f_{pRONO2} values observed at greater nitrate loadings. Instead, higher f_{pRONO2} appears to be related to plume age, with fresh emissions showing a higher fraction (Figure 4c). For instance, at ages less than 1 h, ON accounted for up to 80% of the pNO_3 but <10% after 5 h. As the aging processes continue, f_{pRONO2} increases and approaches nearly 1 for the most aged BB plume sampled at the MBO.

3.2.3. Aging-Induced Transformation of Potassium Species. Potassium is often used as a tracer for BB in the ambient environment.[81,82] Here, K^+ was measured, alongside ions representing potassium salts, including $K_3SO_4^+$, $K_2NO_3^+$, K_2Cl^+, and K_2OH^+. Previous studies noted negligible enhance-

https://doi.org/10.1021/acsestair.5c00002
ACS EST Air 2025, 2, 677−691

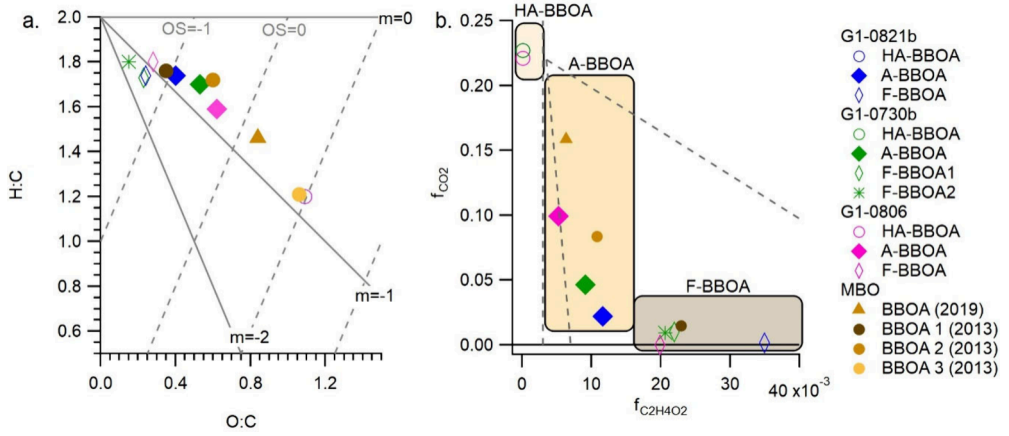

Figure 5. Distributions of the PMF factors within (a) Van Krevelen space and (b) the f_{CO2} (f_{44}) vs the f_{C2H4O2} (f_{60}) space. The factors are grouped into three types, as indicated by the shaded boxes.

ment of K^+ in BB plumes at MBO.[33,36] Similarly, no enhancement was seen during G1-0806, which sampled plumes from similar source regions, confirming the depletion of potassium in wildfire plumes originating from northern California and southern Oregon. This depletion could potentially be attributed to the types of fuels burned. For example, previous studies have shown that montane species like Douglas fir and ponderosa pine emit a lower potassium mass fraction than other fuels types, such as sagebrush.[83,84]

Elevated concentrations of K species were seen during the G1-0730b and G1-0821b samplings. Here we use G1-0730b as a case study to delve into the transformations of potassium salts and the utility of this information regarding the atmospheric aging of BB smoke. During this research flight, approximately 80−90% of the potassium was detected as K^+; however, non-negligible amounts of $K_3SO_4^+$, $K_2NO_3^+$, K_2Cl^+, and K_2OH^+ were also detected (Figure S5). While these compounds have been previously detected with laser-ablation single particle mass spectrometry,[85−87] their detection with SP-AMS was rarely reported.[88]

Quantifying K-containing compounds through AMS measurements is difficult due to the thermal ionization processes occurring on the tungsten vaporizer or on the surface of rBC when the laser vaporizer is utilized.[89] In this study, concentrations of K-containing species are reported in nitrate equivalents (i.e., RIE = 1 and CE = 1). Additionally, the fragmentation pattern of K-containing compounds is unknown. We expect that K compounds are internally mixed with rBC, suggesting that laser vaporization is the dominant ionization process for K^+ adducts. However, we do observe a 0.007 amu shift in the $^{39}K^+$ peak, indicative of the influence of surface ionization, as ions produced through this source traverse a slightly different trajectory within the mass spectrometer.[89]

Most K is emitted in the form of KCl and KOH during biomass combustion.[90] During atmospheric transport, these compounds can undergo acid replacement reactions with H_2SO_4 and HNO_3 to form K_2SO_4 and KNO_3, respectively. The presence of these species was found to increase with longer aging time, although these reactions are dependent on the availability of precursors.[81,87] Additionally, if there is sufficient SO_2(g) present during combustion, K_2SO_4 can be formed directly during the combustion process, especially at high temperatures (>1000 °C).[91,92] These conditions are more likely to be met during flaming combustion, which may explain why previous studies have reported an exponential increase in particulate potassium concentration with modified combustion efficiency (MCE).[93]

Figure S5a shows the changes of each potassium species, normalized by total K signal or CO concentration, with the estimated photochemical age (PCA) during the G1-0730b flight. As expected, K_2Cl^+ shows a rapid decrease with photochemical age, reaching minimal NEMR values ($\Delta K_2Cl^+/\Delta CO$) at PCA > 5 h. The decline of the NEMR of K_2Cl^+ behaved akin to a pseudo-first-order reaction, with an estimated rate constant of 0.37 h^{-1}. A strong dependence is also seen between the NEMR of K_2Cl^+ and oxidation markers such as O/C and f_{44} (Figure S4b). This suggests that K_2Cl^+ may be a useful indicator of transport time in the near-field, although its sensitivity to H_2SO_4 and HNO_3 concentrations remains unknown.

$K_3SO_4^+$ was expected to be a secondary species, but no clear trend with photochemical age was observed (Figure S5). Instead, a strong dependence on sulfate was seen (r^2 = 0.89; Figure S5c), indicating that K_2SO_4 formation may be more strongly related to the concentration of sulfate. It is also possible that this compound has already formed by the time of the first transect or during the combustion process. Although the concentrations of $K_2NO_3^+$ were low, their contribution to total potassium increased with age, consistent with secondary formation.

3.3. Characterization of BBOA Transformation Using Positive Matrix Factorization (PMF). We employed PMF analysis to further probe the transformations of BBOA and gain a better understanding of the primary and secondary organic aerosol components in the wildfire plumes. The spectral characteristics of all PMF factors are shown in Figures S6−S10. The fresh BBOA factors (F-BBOA), representing primary BBOA, exhibit the highest signals at $C_2H_4O_2^+$ and $C_3H_5O_2^+$, both of which are marker ions for levoglucosan and other anhydrosugars (Figure 5). The spread of f_{C2H4O2} values in the fresh BBOA category may indicate the variation in the emission of anhydrosugars during pyrolysis, which can be influenced by the cellulose content of the fuel[31] as well as burning efficiency.[27] All of the F-BBOAs have similar O/C values ranging from 0.15 to 0.26. However, as primary BBOA in wildfire plumes undergoes chemical degradation, their f_{C2H4O2} values converge and appear to be independent of the initial values (HA-BBOA in Figure 5). Although PMF analysis

https://doi.org/10.1021/acsestair.5c00002
ACS EST Air 2025, 2, 677−691

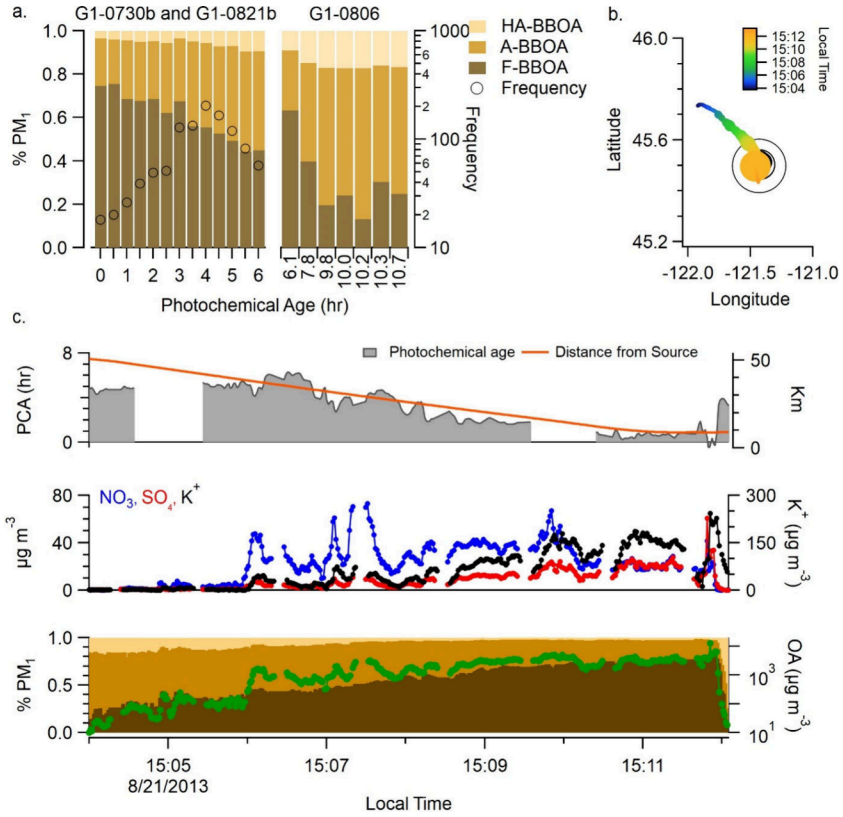

Figure 6. (a) Change in OA composition with photochemical age for the G1 research flights. The left side includes all data points binned by photochemical age, with the frequency corresponding to the number of data points within each bin. The right side corresponds with individual smoke events sampled during G1-0806. (b) Map of the G1 aircraft location during the cross-plume transect during G1-0821b. Aircraft location is shown by circles, colored by sampling time and sized by measured PM_1 concentration. Open black circles indicate thermal anomalies detected by MODIS. (c) Change in inorganic and OA composition during the cross-plume transect during G1-0821.

was conducted separately for each of the G1 aircraft measurements and at the MBO summit site, a comparison of the spectral features provides further insights into the BBOA aging.

While the physical age of a plume represents the duration since its emission, it accounts for both daytime and nighttime transport and is independent of oxidant concentrations. As demonstrated by Zhou et al.,[36] daytime aging of wildfire plumes resulted in significantly more oxidized BBOA compared to those transported during nighttime. Additionally, BBOA in plumes with similar ages may show different degrees of oxidation due to differences in sunlight intensity exposure. For example, Palm et al.[26] have reported enhanced photolysis rates (e.g., j_{HONO}) near the plume edges in comparison with the core. Likewise, as shown in Figure S3, we see much higher photochemical ages on transect edges nearest the source when compared to the plume core, suggesting that the photochemical age metric effectively captures this heterogeneity within the plume. Interestingly, as the plume undergoes dilution, this effect becomes increasingly negligible and eventually reverses, with the plume core showing higher photochemical ages relative to the edges (Figure S3). This may be due to the greater availability of oxidants in the previously optically thick plume.

Figure 6a demonstrates that over the course of atmospheric processing observed during the G1-0730b and G1-0821b flights, the F-BBOA factors show a nearly monotonic decrease in fractional abundance with increasing photochemical age, gradually giving way to the factors representing aged BBOA. This observation suggests that fresh BBOA material is lost via either evaporation or chemical reactions, similar to what is delineated by Sedlacek et al.[19] In plume transects with the lowest photochemical ages, the F-BBOA factors accounted for approximately 75% of the OA mass (Figure 6a). Over the first 10 h of photochemical processing, this fraction decreased to approximately 20%. Most of the remaining mass is attributed to the aged BBOA factor (A-BBOA). However, between 3 and 18% of the total OA mass is attributed to the highly aged BBOA factor (HA-BBOA), suggesting that highly processed BBOA is formed rapidly within the first 10 h of plume aging. Furthermore, the fraction of mass attributed to the HA-BBOA factor is highest near the edges of the plume.

The differences between the F-BBOA factors resolved during each of the research flights may be a result of fuel types with different emission profiles.[14,94] Two fresh BBOA factors were identified during the G1-0730b research flight, and although their spectra share similar f_{60} and f_{44} values, there are key differences. Notably, the fresh BBOA-1 factor exhibits enhanced signals in high m/z C_xH_y ions, such as $C_7H_7^+$ (m/z 91.05), $C_8H_9^+$ (m/z 105.05), $C_9H_7^+$ (m/z 115.06), and $C_{13}H_9^+$ (m/z 165.07), which may indicate the presence of polycyclic aromatic hydrocarbons (PAHs).[95] Additionally, these factors show different temporal patterns consistent with previous analysis that found considerable spatial variation of the chemical composition within this plume.[39]

During G1-0821b, an along-plume transect was conducted, during which the aircraft flew directly from the furthest point away from the fire to the fire epicenter in about 5 min (Figure

https://doi.org/10.1021/acsestair.5c00002
ACS EST Air 2025, 2, 677−691

6b). This transect spans a range of photochemical ages from 0 to 6 h, with OA loadings ranging between 10 and 10^4 μg m^{-3}. Furthermore, the short time frame of the transect helps minimize uncertainties arising from changes in atmospheric conditions during the measurement period. At the furthest point during this transect which has undergone the most atmospheric processing, the F-BBOA factor only accounts for 30% of the total OA, and up to 20% of the OA is attributed to HA-BBOA. However, as the aircraft approached the emission source, the mass fraction of F-BBOA increased to 80%. The mass loading of nitrate peaks downwind of the organic loading peak, highlighting the relatively slow formation of this secondary species.

While both G1-0821b and G1-0730b showed strong correlations between OA and rBC, G1-0821b displayed a much higher ΔOA/ΔrBC in comparison to G1-0730b, with ratios of 30.2 and 14.9, respectively. As both of these fires had similar average MCE values, these differences are likely due to underlying fuel differences. The variations in fuel sources may also have implications for the BBOA composition. For instance, the high f_{60} identified in the fresh BBOA during G1-0821b is consistent with laboratory measurements of grass emissions.[31]

The identification of different fuel types was accomplished using high resolution (30 m × 30 m resolution) vegetation maps from the Landscape Fire and Resource Management Planning Tools (https://landfire.gov/) during the Government Flat fire (G1-0821b) and the Colockum Tarps fire (G1-0730b), as detailed in Section S1.5. Overall, the Government Flat fire primarily consisted of open and closed canopy mixed conifer forests, while the Colockum Tarps fire had a high contribution from shrubland and herbaceous grassland. Although each individual fire covers a wide area and emissions likely result from a mixture of different species, this suggests that the properties of primary BBOA can vary among wildfires in different ecosystems. This distinction is noteworthy when performing source apportionment studies in areas impacted by wildfire smoke, especially when a priori spectral information is used, such as in PMF analysis utilizing Machine Engine 2 (ME-2).[58] However, regardless of the initial POA signature and fuel types, the BBOA for each flight ultimately converged toward a similar composition with processing, as represented by the A-BBOA and HA-BBOA factors.

3.4. Age-Dependent NEMRs in Wildfire Plumes and Role of Dilution-Induced Evaporation in Plume BBOA Processing. Figure 4a provides an overview of the changes in the normalized excess mass ratio of OA relative to that of CO (ΔOA/ΔCO) with plume age for the wildfire plumes observed in this study. Across the G1-0730b and G1-0821b research flights, there is no statistically significant relationship between ΔOA/ΔCO and photochemical age; instead, much of the variability in ΔOA/ΔCO is associated with substantial changes in the OA concentration, spanning 3 orders of magnitude. However, for plumes sampled during G1-0806 and at MBO, ΔOA/ΔCO exhibits a pronounced decreasing trend at a photochemical age greater than 12 h. These findings suggest that within the initial few hours of atmospheric aging, the production of SOA and the loss of BBOA from evaporation, chemical fragmentation, and/or deposition are relatively balanced. However, with extended processing (e.g., >12 h), the loss of aerosol mass becomes more important in comparison to secondary aerosol formation.

To determine the role of evaporation in the change in aerosol mass, we quantified the volatility of each BBOA factor identified at the MBO summit site using mass thermograms measured with a thermodenuder (Figure 7a). Note that no

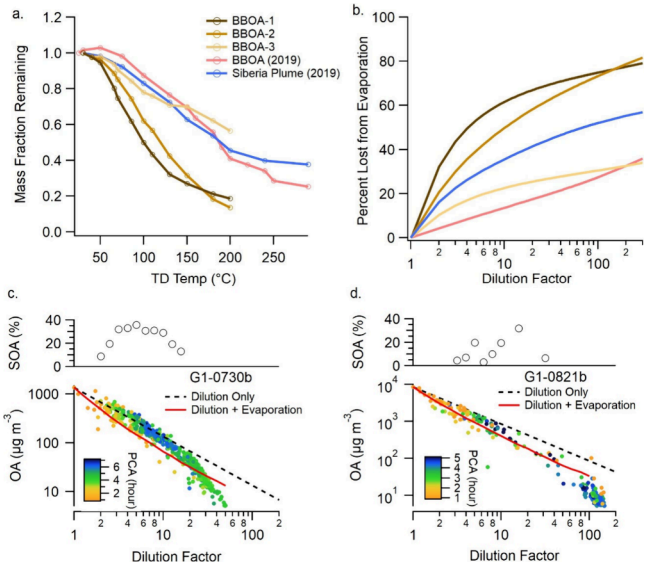

Figure 7. (a) Mass thermograms for the BBOA factors. (b) Percent of OA mass lost through evaporation for each BBOA factor at increasing dilution factors. Change in OA mass with increasing dilution factor during (c) the G1-0730b research flight and (d) the G1-0821b research flight. The dashed line is the expected trend if only dilution is considered, while the red line accounts for evaporative loss in addition to dilution. Black circles indicate the percent of OA mass attributed to SOA in each dilution factor bin.

thermodenuder measurements were conducted aboard the G1 aircraft. As expected from the thermograms, BBOA-1 shows the largest fraction of higher volatility material, peaking at a saturation vapor pressure (C^*) of 10^1 μg m^{-3} (Figure 8). As BBOA ages, the C^* distribution shifts toward lower volatility bins, peaking at 10^{-2} and 10^{-4} μg m^{-3} for BBOA-2 and BBOA-3, respectively. The C^* distribution for the BBOA factor identified in MBO-2019 exhibits a peak at 10^{-3} μg m^{-3}, accompanied by a significant contribution from components

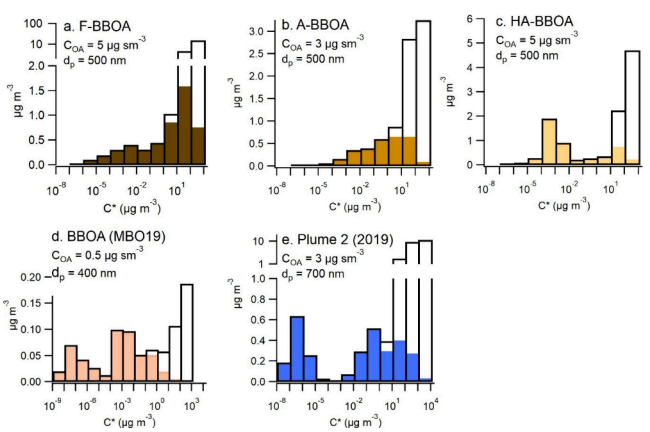

Figure 8. Volatility distribution corresponding to 298 K of the BBOA factors identified in Zhou et al.[36] and Farley et al.[33] The colored bars correspond with the particle-phase fraction, while the black boxes correspond with the total gas and particle-phase concentration.

https://doi.org/10.1021/acsestair.5c00002
ACS EST Air 2025, 2, 677−691

with C^* as low as 10^{-8} $\mu g\ m^{-3}$, indicative of extensive atmospheric processing (Figure 8d). Additionally, Figure 8e shows the OA volatility during a highly processed wildfire plume transported from Siberia with an estimated aging time of about 2 weeks. In this event, the C^* distribution shows a considerable amount of OA mass at $C^* < 10^{-6}$ $\mu g\ m^{-3}$. The concurrent presence of higher volatility material could indicate the formation of more volatile species through chemical aging or mixing with more volatile non-BB aerosol during atmospheric transport.

Using the volatility distribution of each BBOA factor, we calculated the amount of particle mass lost through evaporation under different degrees of plume dilution (Figure 7b). Upon mixing with clean background air up to a dilution factor of 200, both the fresh BBOA-1 and the moderately aged BBOA-2 show up to 80% mass loss from evaporation. In contrast, the more extensively aged BBOAs, including the highly aged BBOA-3, the 2019 BBOA factor, and the Siberia BBOA plume, show evaporative losses that are approximately half as low. Although similar thermal profiles are seen in Figure 7a for these aged BBOA species, they show different behavior upon dilution due to different levels of aerosol loading.

For the G1-0730b and G1-0821b research flights, we calculated the dilution factor at time point i as $[CO_{max}]/[CO_i]$, where $[CO_{max}]$ is the highest CO concentration measured during the flight. The dilution factor increases with photochemical age, especially for time points with high organic aerosol loading, while the trend becomes less clear as CO approaches background concentrations (Figure S13). When plotted against the dilution factor, the OA concentration shows a decreasing trend due to mixing with background air. If no evaporative loss or SOA formation occurs, then the data points should fall along a straight line, indicated by the black dashed lines in Figure 7c,d.

The red lines in Figure 7c,d depict the predicted change of the BBOA concentration assuming both dilution and evaporation. The evaporation is estimated based on bulk OA volatility calculated using the composition determined by PMF analysis. The measured OA concentrations are generally higher than those predictions if both dilution and evaporation are accounted for, indicating substantial formation of SOA material. To estimate the contribution of SOA to total OA mass, we calculated the differences between the measured OA concentrations and the predicted OA concentrations after accounting for evaporative loss. This fraction ranges from 20 to 40% at dilution factors between 5 and 10 (Figure 7c,d). At higher dilution factors, the observed OA mass concentrations fall significantly below the predicted trend lines, indicating significant BBOA loss processes such as chemical degradation or deposition during extended atmospheric aging.

Leveraging observations from both aerial and mountaintop platforms, we comprehensively examined wildfire plumes in the Pacific Northwest spanning a wide range of processing stages, from near-field plumes to those subjected to regional and intercontinental transport. Photochemical age was calculated for fresh and intermediately aged plumes based on the decay of NO_x relative to CO. This metric offers a reliable estimate of physical transport time while revealing fine-scale variations within the plumes driven by spatiotemporal variations in oxidant concentrations. However, this metric is not applicable for heavily processed plumes in which the NO_x concentrations have returned to background levels. In such cases, estimating physical transport time based on travel distance from the source—such as through the comparison of modeled back trajectories and satellite thermal anomalies—may be more useful for characterizing the age of plumes older than 12 h since emission. We successfully identified distinct BBOA signatures representing varying degrees of processing in wildfire plumes. Notably, there was a rapid decrease in the mass fraction of fresh BBOA factors, characterized by low O/C values (0.15−0.26), as they were gradually replaced by more oxidized aerosol with aging. This transformation can be attributed to a combination of the volatilization of the more volatile fresh BBOA and the formation of less volatile, more oxidized secondary BBOAs. Furthermore, a rapid formation of highly oxidized BBOA types, with an average O/C as high as 1.06, was observed within the first 6 to 12 h of photochemical processing. Utilizing direct measurements of aerosol volatility, we estimate that within the first few hours of plume processing, up to 40% of OA mass was secondary. The chemical modifications of the OA in wildfire smoke correspond to changes in microphysical and optical properties. Aged BBOA is likely more hydrophilic and can act more effectively as cloud condensation nuclei (CCN), thereby altering cloud properties in remote regions, such as over the oceans and in the Arctic.[96−98] Furthermore, the coating of BB-derived SOA onto black carbon aerosol has been shown to enhance the absorption of radiation.[99] These results highlight the importance of accurately representing the evolution processes of BBOA, considering both mass concentrations and chemical properties, in the atmosphere to properly assess the environmental and climatic impacts of wildfire emissions.

■ ASSOCIATED CONTENT

Supporting Information

The Supporting Information is available free of charge at https://pubs.acs.org/doi/10.1021/acsestair.5c00002.

BBOP and SP-AMS measurements, PMF analysis, photochemical age calculation and comparison with physical transport time, BBOA volatility quantification, wildfire fuel type identification, additional PCA data, sensitivity analysis, flight tracking data, K species data, mass spectra, maps of fires, and comparison tables (PDF)

■ AUTHOR INFORMATION

Corresponding Author

Qi Zhang − *Department of Environmental Toxicology, University of California, Davis, California 95616, United States; Agricultural and Environmental Chemistry Graduate Program and Atmospheric Science Graduate Program, University of California, Davis, California 95616, United States;* orcid.org/0000-0002-5203-8778; Phone: (530)-752-5779; Email: dkwzhang@ucdavis.edu

Authors

Ryan Farley − *Department of Environmental Toxicology, University of California, Davis, California 95616, United States; Agricultural and Environmental Chemistry Graduate Program, University of California, Davis, California 95616, United States;* Present Address: Earth and Environmental Sciences Division, Los Alamos National Laboratory, Los Alamos, New Mexico 87545, United States

Shan Zhou − *Department of Environmental Toxicology, University of California, Davis, California 95616, United*

https://doi.org/10.1021/acsestair.5c00002
ACS EST Air 2025, 2, 677−691

States; Atmospheric Science Graduate Program, University of California, Davis, California 95616, United States; Present Address: College of Engineering, Eastern Institute of Technology, Ningbo, Zhejiang 315048, China

Sonya Collier − *Department of Environmental Toxicology, University of California, Davis, California 95616, United States;* Present Address: California Air Resources Board, 1001 I Street, Sacramento, California 95814, United States

Wenqing Jiang − *Department of Environmental Toxicology, University of California, Davis, California 95616, United States; Agricultural and Environmental Chemistry Graduate Program, University of California, Davis, California 95616, United States;* orcid.org/0000-0002-6869-3232

Timothy B. Onasch − *Aerodyne Research Inc., Billerica, Massachusetts 01821, United States;* orcid.org/0000-0001-7796-7840

John E. Shilling − *Atmospheric, Climate, and Earth Sciences Division, Pacific Northwest National Laboratory, Richland, Washington 99352, United States;* orcid.org/0000-0002-3728-0195

Lawrence Kleinman − *Environmental and Climate Sciences, Brookhaven National Laboratory, Upton, New York 11973, United States*

Arthur J. Sedlacek III − *Environmental and Climate Sciences, Brookhaven National Laboratory, Upton, New York 11973, United States;* orcid.org/0000-0001-9595-3653

Complete contact information is available at: https://pubs.acs.org/10.1021/acsestair.5c00002

Notes

The authors declare no competing financial interest.

■ ACKNOWLEDGMENTS

This work was funded by the U.S. Department of Energy (DOE) Office of Science, Office of Biological and Environmental Research (BER) through the Atmospheric System Research (ASR) program (DE-SC0022140 and DE-SC0014620). R.F. acknowledges funding from the Jastro-Shields Research Award and the Donald G. Crosby Fellowship in Environmental Chemistry from UC Davis. Aircraft measurements used in this study were provided by the Atmospheric Radiation Measurement (ARM) Climate Research Facility, a DOE user facility sponsored by BER. The Pacific Northwest National Laboratory (PNNL) is operated for DOE by Battelle Memorial Institute under Contract DE-AC06-76RL01830.

■ REFERENCES

(1) Jaffe, D. A.; O'Neill, S. M.; Larkin, N. K.; Holder, A. L.; Peterson, D. L.; Halofsky, J. E.; Rappold, A. G. Wildfire and Prescribed Burning Impacts on Air Quality in the United States. *J. Air Waste Manage. Assoc.* **2020**, *70* (6), 583−615.

(2) IPCC. *Climate Change 2021: The Physical Science Basis. Contribution of Working Group I to the Sixth Assessment Report of the Intergovernmental Panel on Climate Change*; Masson-Delmotte, V., Zhai, P., Pirani, A., Connors, S. L., Pean, C., Berger, S., Caud, N., Chen, Y., Goldfarb, L., Gomis, M. I., Huang, M., Leitzell, K., Lonnoy, E., Matthews, J. B., Maycock, T. K., Waterfield, T., Yelekci, O., Yu, R., Zhou, B., Eds.; Cambridge University Press, United Kingdom and New York, NY, USA, 2021. DOI: 10.1017/9781009157896.

(3) Holm, S. M.; Miller, M. D.; Balmes, J. R. Health Effects of Wildfire Smoke in Children and Public Health Tools: A Narrative Review. *J. Expo. Sci. Environ. Epidemiol.* **2021**, *31* (1), 1−20.

(4) Reid, C. E.; Brauer, M.; Johnston, F. H.; Jerrett, M.; Balmes, J. R.; Elliott, C. T. Critical Review of Health Impacts of Wildfire Smoke Exposure. *Environ. Health Perspect.* **2016**, *124* (9), 1334−1343.

(5) Schill, G. P.; Froyd, K. D.; Bian, H.; Kupc, A.; Williamson, C.; Brock, C. B.; Ray, E.; Hornbrook, R. S.; Hills, A. J.; Apel, E. C.; Chin, M.; Colarco, P. R.; Murphy, D. M. Widespread Biomass Burning Smoke throughout the Remote Troposphere. *Nat. Geosci.* **2020**, *13*, 422−427.

(6) O'Dell, K.; Ford, B.; Fischer, E. V.; Pierce, J. R. Contribution of Wildland-Fire Smoke to US PM2.5 and Its Influence on Recent Trends. *Environ. Sci. Technol.* **2019**, *53* (4), 1797−1804.

(7) Jolly, W. M.; Cochrane, M. A.; Freeborn, P. H.; Holden, Z. A.; Brown, T. J.; Williamson, G. J.; Bowman, D. M. J. S. Climate-Induced Variations in Global Wildfire Danger from 1979 to 2013. *Nat. Commun.* **2015**, *6* (May), 1−11.

(8) McClure, C. D.; Jaffe, D. A. Investigation of High Ozone Events Due to Wildfire Smoke in an Urban Area. *Atmos. Environ.* **2018**, *194*, 146−157.

(9) Westerling, A. L.R. Increasing Western US Forest Wildfire Activity: Sensitivity to Changes in the Timing of Spring. *Philos. Trans. R. Soc. B Biol. Sci.* **2016**, *371* (1696), 20150178.

(10) Andreae, M. O. Emission of Trace Gases and Aerosols from Biomass Burning - An Updated Assessment. *Atmos. Chem. Phys.* **2019**, *19* (13), 8523−8546.

(11) May, A. A.; McMeeking, G. R.; Lee, T.; Taylor, J. W.; Craven, J. S.; Burling, I. R.; Sullivan, A. P.; Akagi, S. K.; Collett, J. L.; Flynn, M. J.; Coe, H.; Urbanski, S. P.; Seinfeld, J. H.; Yokelson, R. J.; Kreidenweis, S. M. Aerosol Emissions from Prescribed Fires in the United States: A Synthesis of Laboratory and Aircraft Measurements. *J. Geophys. Res. Atmos.* **2014**, *119* (20), 11826.

(12) Jorga, S. D.; Florou, K.; Kaltsonoudis, C.; Kodros, J. K.; Vasilakopoulou, C.; Cirtog, M.; Fouqueau, A.; Picquet-Varrault, B.; Nenes, A.; Pandis, S. N. Nighttime Chemistry of Biomass Burning Emissions in Urban Areas: A Dual Mobile Chamber Study. *Atmos. Chem. Phys.* **2021**, *21* (19), 15337−15349.

(13) Coggon, M. M.; Lim, C. Y.; Koss, A. R.; Sekimoto, K.; Yuan, B.; Gilman, J. B.; Hagan, D. H.; Selimovic, V.; Zarzana, K. J.; Brown, S. S.; Roberts, J. M.; Müller, M.; Yokelson, R.; Wisthaler, A.; Krechmer, J. E.; Jimenez, J. L.; Cappa, C.; Kroll, J. H.; De Gouw, J.; Warneke, C. OH Chemistry of Non-Methane Organic Gases (NMOGs) Emitted from Laboratory and Ambient Biomass Burning Smoke: Evaluating the Influence of Furans and Oxygenated Aromatics on Ozone and Secondary NMOG Formation. *Atmos. Chem. Phys.* **2019**, *19* (23), 14875−14899.

(14) Ahern, A. T.; Robinson, E. S.; Tkacik, D. S.; Saleh, R.; Hatch, L. E.; Barsanti, K. C.; Stockwell, C. E.; Yokelson, R. J.; Presto, A. A.; Robinson, A. L.; Sullivan, R. C.; Donahue, N. M. Production of Secondary Organic Aerosol During Aging of Biomass Burning Smoke From Fresh Fuels and Its Relationship to VOC Precursors. *J. Geophys. Res. Atmos.* **2019**, *124* (6), 3583−3606.

(15) Jimenez, J. L.; Canagaratna, M. R.; Donahue, N. M.; Prevot, A. S. H.; Zhang, Q.; Kroll, J. H.; DeCarlo, P. F.; Allan, J. D.; Coe, H.; Ng, N. L.; Aiken, A. C.; Docherty, K. S.; Ulbrich, I. M.; Grieshop, A. P.; Robinson, A. L.; Duplissy, J.; Smith, J. D.; Wilson, K. R.; Lanz, V. A.; Hueglin, C.; Sun, Y. L.; Tian, J.; Laaksonen, A.; Raatikainen, T.; Rautiainen, J.; Vaattovaara, P.; Ehn, M.; Kulmala, M.; Tomlinson, J. M.; Collins, D. R.; Cubison, M. J.; Dunlea, E. J.; Huffman, J. A.; Onasch, T. B.; Alfarra, M. R.; Williams, P. I.; Bower, K.; Kondo, Y.; Schneider, J.; Drewnick, F.; Borrmann, S.; Weimer, S.; Demerjian, K.; Salcedo, D.; Cottrell, L.; Griffin, R.; Takami, A.; Miyoshi, T.; Hatakeyama, S.; Shimono, A.; Sun, J. Y.; Zhang, Y. M.; Dzepina, K.; Kimmel, J. R.; Sueper, D.; Jayne, J. T.; Herndon, S. C.; Trimborn, A. M.; Williams, L. R.; Wood, E. C.; Middlebrook, A. M.; Kolb, C. E.; Baltensperger, U.; Worsnop, D. R. Evolution of Organic Aerosols in the Atmosphere. *Science (80-.).* **2009**, *326* (5959), 1525−1529.

(16) Che, H.; Segal-Rozenhaimer, M.; Zhang, L.; Dang, C.; Zuidema, P.; Dobracki, A.; Sedlacek, A. J.; Coe, H.; Wu, H.; Taylor, J.; Zhang, X.; Redemann, J.; Haywood, J. Cloud Processing and Weeklong Ageing Affect Biomass Burning Aerosol Properties

over the South-Eastern Atlantic. *Commun. Earth Environ.* **2022**, *3*, 1−9.
(17) Jiang, W.; Misovich, M. V.; Hettiyadura, A. P. S.; Laskin, A.; McFall, A. S.; Anastasio, C.; Zhang, Q. Photosensitized Reactions of a Phenolic Carbonyl from Wood Combustion in the Aqueous Phase - Chemical Evolution and Light Absorption Properties of AqSOA. *Environ. Sci. Technol.* **2021**, *55* (8), 5199−5211.
(18) Yu, L.; Smith, J.; Laskin, A.; George, K. M.; Anastasio, C.; Laskin, J.; Dillner, A. M.; Zhang, Q. Molecular Transformations of Phenolic SOA during Photochemical Aging in the Aqueous Phase: Competition among Oligomerization, Functionalization, and Fragmentation. *Atmos. Chem. Phys.* **2016**, *16* (7), 4511−4527.
(19) Sedlacek, A. J.; Lewis, E. R.; Onasch, T. B.; Zuidema, P.; Redemann, J.; Jaffe, D.; Kleinman, L. I. Using the Black Carbon Particle Mixing State to Characterize the Lifecycle of Biomass Burning Aerosols. *Environ. Sci. Technol.* **2022**, *56* (20), 14315−14325.
(20) Palm, B. B.; Peng, Q.; Fredrickson, C. D.; Lee, B. H.; Garofalo, L. A.; Pothier, M. A.; Kreidenweis, S. M.; Farmer, D. K.; Pokhrel, R. P.; Shen, Y.; Murphy, S. M.; Permar, W.; Hu, L.; Campos, T. L.; Hall, S. R.; Ullmann, K.; Zhang, X.; Flocke, F.; Fischer, E. V.; Thornton, J. A. Quantification of Organic Aerosol and Brown Carbon Evolution in Fresh Wildfire Plumes. *Proc. Natl. Acad. Sci. U.S.A.* **2020**, *117* (47), 29469−29477.
(21) Forrister, H.; Liu, J.; Scheuer, E.; Dibb, J.; Ziemba, L.; Thornhill, K. L.; Anderson, B.; Diskin, G.; Perring, A. E.; Schwarz, J. P.; Campuzano-Jost, P.; Day, D. A.; Palm, B. B.; Jimenez, J. L.; Nenes, A.; Weber, R. J. Evolution of Brown Carbon in Wildfire Plumes. *Geophys. Res. Lett.* **2015**, *42* (11), 4623−4630.
(22) Lambe, A. T.; Onasch, T. B.; Massoli, P.; Croasdale, D. R.; Wright, J. P.; Ahern, A. T.; Williams, L. R.; Worsnop, D. R.; Brune, W. H.; Davidovits, P. Laboratory Studies of the Chemical Composition and Cloud Condensation Nuclei (CCN) Activity of Secondary Organic Aerosol (SOA) and Oxidized Primary Organic Aerosol (OPOA). *Atmos. Chem. Phys.* **2011**, *11* (17), 8913−8928.
(23) Donahue, N. M.; Robinson, A. L.; Stanier, C. O.; Pandis, S. N. Coupled Partitioning, Dilution, and Chemical Aging of Semivolatile Organics. *Environ. Sci. Technol.* **2006**, *40* (8), 2635−2643.
(24) Hodshire, A. L.; Ramnarine, E.; Akherati, A.; Alvarado, M. L.; Farmer, D. K.; Jathar, H.; Kreidenweis, S. M.; Lonsdale, C. R.; Onasch, T. B.; Springston, S. R.; et al. Dilution Impacts on Smoke Aging: Evidence in Biomass Burning Observation Project (BBOP) Data. *Atmos. Chem. Phys.* **2021**, *21* (9), 6839−6855.
(25) June, N. A.; Hodshire, A. L.; Wiggins, E. B.; Winstead, E. L.; Robinson, C. E.; Thornhill, K. L.; Sanchez, K. J.; Moore, R. H.; Pagonis, D.; Guo, H.; Campuzano-Jost, P.; Jimenez, J. L.; Coggon, M. M.; Dean-Day, J. M.; Bui, T. P.; Peischl, J.; Yokelson, R. J.; Alvarado, M. J.; Kreidenweis, S. M.; Jathar, S. H.; Pierce, J. R. Aerosol Size Distribution Changes in FIREX-AQ Biomass Burning Plumes: The Impact of Plume Concentration on Coagulation and OA Condensation/Evaporation. *Atmos. Chem. Phys.* **2022**, *22* (19), 12803−12825.
(26) Palm, B. B.; Peng, Q.; Hall, S. R.; Ullmann, K.; Campos, T. L.; Weinheimer, A.; Montzka, D.; Tyndall, G.; Permar, W.; Hu, L.; Flocke, F.; Fischer, E. V.; Thornton, J. A. Spatially Resolved Photochemistry Impacts Emissions Estimates in Fresh Wildfire Plumes. *Geophys. Res. Lett.* **2021**, *48* (23), e2021GL095443.
(27) Collier, S.; Zhou, S.; Onasch, T. B.; Jaffe, D. A.; Kleinman, L.; Sedlacek, A. J.; Briggs, N. L.; Hee, J.; Fortner, E.; Shilling, J. E.; Worsnop, D.; Yokelson, R. J.; Parworth, C.; Ge, X.; Xu, J.; Butterfield, Z.; Chand, D.; Dubey, M. K.; Pekour, M. S.; Springston, S.; Zhang, Q. Regional Influence of Aerosol Emissions from Wildfires Driven by Combustion Efficiency: Insights from the BBOP Campaign. *Environ. Sci. Technol.* **2016**, *50* (16), 8613−8622.
(28) Ortega, A. M.; Day, D. A.; Cubison, M. J.; Brune, W. H.; Bon, D.; De Gouw, J. A.; Jimenez, J. L. Secondary Organic Aerosol Formation and Primary Organic Aerosol Oxidation from Biomass-Burning Smoke in a Flow Reactor during FLAME-3. *Atmos. Chem. Phys.* **2013**, *13* (22), 11551−11571.
(29) Hodshire, A. L.; Akherati, A.; Alvarado, M. J.; Brown-Steiner, B.; Jathar, S. H.; Jimenez, J. L.; Kreidenweis, S. M.; Lonsdale, C. R.; Onasch, T. B.; Ortega, A. M.; Pierce, J. R. Aging Effects on Biomass Burning Aerosol Mass and Composition: A Critical Review of Field and Laboratory Studies. *Environ. Sci. Technol.* **2019**, *53* (17), 10007−10022.
(30) Yokelson, R. J.; Crounse, J. D.; DeCarlo, P. F.; Karl, T.; Urbanski, S.; Atlas, E.; Campos, T.; Shinozuka, Y.; Kapustin, V.; Clarke, A. D.; Weinheimer, A.; Knapp, D. J.; Montzka, D. D.; Holloway, J.; Weibring, P.; Flocke, F.; Zheng, W.; Toohey, D.; Wennberg, P. O.; Wiedinmyer, C.; Mauldin, L.; Fried, A.; Richter, D.; Walega, J.; Jimenez, J. L.; Adachi, K.; Buseck, P. R.; Hall, S. R.; Shetter, R. Emissions from Biomass Burning in the Yucatan. *Atmos. Chem. Phys.* **2009**, *9* (15), 5785−5812.
(31) Cubison, M. J.; Ortega, A. M.; Hayes, P. L.; Farmer, D. K.; Day, D.; Lechner, M. J.; Brune, W. H.; Apel, E.; Diskin, G. S.; Fisher, J. A.; Fuelberg, H. E.; Hecobian, A.; Knapp, D. J.; Mikoviny, T.; Riemer, D.; Sachse, G. W.; Sessions, W.; Weber, R. J.; Weinheimer, A. J.; Wisthaler, A.; Jimenez, J. L. Effects of Aging on Organic Aerosol from Open Biomass Burning Smoke in Aircraft and Laboratory Studies. *Atmos. Chem. Phys.* **2011**, *11* (23), 12049−12064.
(32) Akagi, S. K.; Craven, J. S.; Taylor, J. W.; McMeeking, G. R.; Yokelson, R. J.; Burling, I. R.; Urbanski, S. P.; Wold, C. E.; Seinfeld, J. H.; Coe, H.; Alvarado, M. J.; Weise, D. R. Evolution of Trace Gases and Particles Emitted by a Chaparral Fire in California. *Atmos. Chem. Phys.* **2012**, *12* (3), 1397−1421.
(33) Farley, R.; Bernays, N.; Jaffe, D. A.; Ketcherside, D.; Hu, L.; Zhou, S.; Collier, S.; Zhang, Q. Persistent Influence of Wildfire Emissions in the Western United States and Characteristics of Aged Biomass Burning Organic Aerosols under Clean Air Conditions. *Environ. Sci. Technol.* **2022**, *56* (6), 3645−3657.
(34) Garofalo, L. A.; Pothier, M. A.; Levin, E. J. T.; Campos, T.; Kreidenweis, S. M.; Farmer, D. K. Emission and Evolution of Submicron Organic Aerosol in Smoke from Wildfires in the Western United States. *ACS Earth Sp. Chem.* **2019**, *3* (7), 1237−1247.
(35) Wu, H.; Taylor, J. W.; Langridge, J. M.; Yu, C.; Allan, J. D.; Szpek, K.; Cotterell, M. I.; Williams, P. I.; Flynn, M.; Barker, P.; Fox, C.; Allen, G.; Lee, J.; Coe, H. Rapid Transformation of Ambient Absorbing Aerosols from West African Biomass Burning. *Atmos. Chem. Phys.* **2021**, *21* (12), 9417−9440.
(36) Zhou, S.; Collier, S.; Jaffe, D. A.; Briggs, N. L.; Hee, J.; Sedlacek III, A. J.; Kleinman, L.; Onasch, T. B.; Zhang, Q. Regional Influence of Wildfires on Aerosol Chemistry in the Western US and Insights into Atmospheric Aging of Biomass Burning Organic Aerosol. *Atmos. Chem. Phys.* **2017**, *17* (3), 2477.
(37) May, A. A.; Lee, T.; McMeeking, G. R.; Akagi, S.; Sullivan, A. P.; Urbanski, S.; Yokelson, R. J.; Kreidenweis, S. M. Observations and Analysis of Organic Aerosol Evolution in Some Prescribed Fire Smoke Plumes. *Atmos. Chem. Phys.* **2015**, *15* (11), 6323−6335.
(38) Akherati, A.; He, Y.; Garofalo, L. A.; Hodshire, A. L.; Farmer, D. K.; Kreidenweis, S. M.; Permar, W.; Hu, L.; Fischer, E. V.; Jen, C. N.; Goldstein, A. H.; Levin, E. J. T.; DeMott, P. J.; Campos, T. L.; Flocke, F.; Reeves, J. M.; Toohey, D. W.; Pierce, J. R.; Jathar, S. H. Dilution and Photooxidation Driven Processes Explain the Evolution of Organic Aerosol in Wildfire Plumes. *Environ. Sci. Atmos.* **2022**, *2* (5), 1000.
(39) Kleinman, L.; Sedlacek, A., III; Adachi, K.; Buseck, P.; Collier, S.; Dubey, M.; Hodshire, A.; Lewis, E.; Onasch, T.; Pierce, J.; Shilling, J.; Springston, S.; Wang, J.; Zhang, Q.; Zhou, S.; Yokelson, R. Rapid Evolution of Aerosol Particles and Their Optical Properties Downwind of Wildfires in the Western U.S. *Atmos. Chem. Phys.* **2020**, *20* (21), 13319−13341.
(40) Permar, W.; Wang, Q.; Selimovic, V.; Wielgasz, C.; Yokelson, R. J.; Hornbrook, R. S.; Hills, A. J.; Apel, E. C.; Ku, I. T.; Zhou, Y.; Sive, B. C.; Sullivan, A. P.; Collett, J. L.; Campos, T. L.; Palm, B. B.; Peng, Q.; Thornton, J. A.; Garofalo, L. A.; Farmer, D. K.; Kreidenweis, S. M.; Levin, E. J. T.; DeMott, P. J.; Flocke, F.; Fischer, E. V.; Hu, L. Emissions of Trace Organic Gases From

https://doi.org/10.1021/acsestair.5c00002
ACS EST Air 2025, 2, 677−691

Western U.S. Wildfires Based on WE-CAN Aircraft Measurements. *J. Geophys. Res. Atmos.* **2021**, *126* (11), 1−29.
(41) Morgan, W. T.; Allan, J. D.; Bauguitte, S.; Darbyshire, E.; Flynn, M. J.; Lee, J.; Liu, D.; Johnson, B.; Haywood, J.; Longo, K. M.; Artaxo, P. E.; Coe, H. Transformation and Ageing of Biomass Burning Carbonaceous Aerosol over Tropical South America from Aircraft in Situ Measurements during SAMBBA. *Atmos. Chem. Phys.* **2020**, *20* (9), 5309−5326.
(42) Capes, G.; Johnson, B.; Mcfiggans, G.; Williams, P. I.; Haywood, J.; Coe, H. Aging of Biomass Burning Aerosols over West Africa: Aircraft Measurements of Chemical Composition, Microphysical Properties, and Emission Ratios. *J. Geo* **2008**, *113*, 1−13.
(43) Zhang, Q.; Zhou, S.; Collier, S.; Jaffe, D.; Onasch, T.; Shilling, J.; Kleinman, L.; Sedlacek, A. Understanding Composition, Formation, and Aging of Organic Aerosols in Wildfire Emissions via Combined Mountain Top and Airborne Measurements. *ACS Symp. Ser.* **2018**, *1299*, 363−385.
(44) Dzepina, K.; Mazzoleni, C.; Fialho, P.; China, S.; Zhang, B.; Owen, R. C.; Helmig, D.; Hueber, J.; Kumar, S.; Perlinger, J. A.; Kramer, L. J.; Dziobak, M. P.; Ampadu, M. T.; Olsen, S.; Wuebbles, D. J.; Mazzoleni, L. R. Molecular Characterization of Free Tropospheric Aerosol Collected at the Pico Mountain Observatory: A Case Study with a Long-Range Transported Biomass Burning Plume. *Atmos. Chem. Phys.* **2015**, *15* (9), 5047−5068.
(45) Lee, J. Y.; Peterson, P. K.; Vear, L. R.; Cook, R. D.; Sullivan, A. P.; Smith, E.; Hawkins, L. N.; Olson, N. E.; Hems, R.; Snyder, P. K.; Pratt, K. A. Wildfire Smoke Influence on Cloud Water Chemical Composition at Whiteface Mountain, New York. *JGR Atmospheres* **2022**, *127*, e2022JD037177.
(46) Young, D. E.; Kim, H.; Parworth, C.; Zhou, S.; Zhang, X.; Cappa, C. D.; Seco, R.; Kim, S.; Zhang, Q. Influences of Emission Sources and Meteorology on Aerosol Chemistry in a Polluted Urban Environment: Results from DISCOVER-AQ California. *Atmos. Chem. Phys.* **2016**, *16* (8), 5427−5451.
(47) Paglione, M.; Gilardoni, S.; Rinaldi, M.; Decesari, S.; Zanca, N.; Sandrini, S.; Giulianelli, L.; Bacco, D.; Ferrari, S.; Poluzzi, V.; Scotto, F.; Trentini, A.; Poulain, L.; Herrmann, H.; Wiedensohler, A.; Canonaco, F.; Prévôt, A. S. H.; Massoli, P.; Carbone, C.; Facchini, M. C.; Fuzzi, S. The Impact of Biomass Burning and Aqueous-Phase Processing on Air Quality: A Multi-Year Source Apportionment Study in the Po Valley, Italy. *Atmos. Chem. Phys.* **2020**, *20* (3), 1233−1254.
(48) Brito, J.; Rizzo, L. V.; Morgan, W. T.; Coe, H.; Johnson, B.; Haywood, J.; Longo, K.; Freitas, S.; Andreae, M. O.; Artaxo, P. Ground-Based Aerosol Characterization during the South American Biomass Burning Analysis (SAMBBA) Field Experiment. *Atmos. Chem. Phys.* **2014**, *14* (22), 12069−12083.
(49) Kleinman, L.; Sedlacek III, A. J. In *Biomass Burning Observation Project (BBOP) Final Campaign Report*; U.S. Department of Energy, 2016. DOI: 10.2172/1236490.
(50) Baylon, P.; Jaffe, D. A.; de Gouw, J.; Warneke, C. Influence of Long-Range Transport of Siberian Biomass Burning at the Mt. Bachelor Observatory during the Spring of 2015. *Aerosol Air Qual. Res.* **2017**, *17* (11), 2751−2761.
(51) Zhang, L.; Jaffe, D. A. Trends and Sources of Ozone and Sub-Micron Aerosols at the Mt. Bachelor Observatory (MBO) during 2004−2015. *Atmos. Environ.* **2017**, *165*, 143−154.
(52) May, N. W.; Bernays, N.; Farley, R.; Zhang, Q.; Jaffe, D. A. Intensive Aerosol Properties of Boreal and Regional Biomass Burning Aerosol at Mt. Bachelor Observatory: Larger and Black Carbon (BC)-Dominant Particles Transported from Siberian Wildfires. *Atmos. Chem. Phys.* **2023**, *23*, 2747−2764.
(53) Zhou, S.; Collier, S.; Jaffe, D. A.; Zhang, Q. Free Tropospheric Aerosols at the Mt. Bachelor Observatory: More Oxidized and Higher Sulfate Content Compared to Boundary Layer Aerosols. *Atmos. Chem. Phys.* **2019**, *19* (3), 1571−1585.
(54) Sedlacek, A. J.; Buseck, P. R.; Adachi, K.; Onasch, T. B.; Springston, S. R.; Kleinman, L. Formation and Evolution of Tar Balls from Northwestern US Wildfires. *Atmos. Chem. Phys.* **2018**, *18* (15), 11289−11301.
(55) Wigder, N. L.; Jaffe, D. A.; Saketa, F. A. Ozone and Particulate Matter Enhancements from Regional Wildfires Observed at Mount Bachelor during 2004−2011. *Atmos. Environ.* **2013**, *75*, 24−31.
(56) Paatero, P.; Tapper, U. Positive Matrix Factorization: A Non-negative Factor Model with Optimal Utilization of Error Estimates of Data Values. *Environmetrics* **1994**, *5* (2), 111−126.
(57) Ulbrich, I. M.; Canagaratna, M. R.; Zhang, Q.; Worsnop, D. R.; Jimenez, J. L. Interpretation of Organic Components from Positive Matrix Factorization of Aerosol Mass Spectrometric Data. *Atmos. Chem. Phys.* **2009**, *9* (9), 2891−2918.
(58) Canonaco, F.; Crippa, M.; Slowik, J. G.; Baltensperger, U.; Prévôt, A. S. H. SoFi, an IGOR-Based Interface for the Efficient Use of the Generalized Multilinear Engine (ME-2) for the Source Apportionment: ME-2 Application to Aerosol Mass Spectrometer Data. *Atmos. Meas. Technol.* **2013**, *6* (12), 3649−3661.
(59) Weiss-Penzias, P.; Jaffe, D. A.; Swartzendruber, P.; Dennison, J. B.; Chand, D.; Hafner, W.; Prestbo, E. Observations of Asian Air Pollution in the Free Troposphere at Mount Bachelor Observatory during the Spring of 2004. *J. Geophys. Res. Atmos.* **2006**, *111* (D10), 1.
(60) Seinfeld, J. H.; Pandis, S. N. In *Atmospheric Chemistry and Physics: From Air Pollution to Climate Change*, 2nd ed.; Wiley Interscience, 2006. DOI: 10.1063/1.882420.
(61) Simpson, I. J.; Akagi, S. K.; Barletta, B.; Blake, N. J.; Choi, Y.; Diskin, G. S.; Fried, A.; Fuelberg, H. E.; Meinardi, S.; Rowland, F. S.; Vay, S. A.; Weinheimer, A. J.; Wennberg, P. O.; Wiebring, P.; Wisthaler, A.; Yang, M.; Yokelson, R. J.; Blake, D. R. Boreal Forest Fire Emissions in Fresh Canadian Smoke Plumes: C1-C10 Volatile Organic Compounds (VOCs), CO2, CO, NO2, NO, HCN and CH3CN. *Atmos. Chem. Phys.* **2011**, *11*, 6445−6463.
(62) Burling, I. R.; Yokelson, R. J.; Griffith, D. W. T.; Johnson, T. J.; Veres, P.; Roberts, J. M.; Warneke, C.; Urbanski, S. P.; Reardon, J.; Weise, D. R.; Hao, W. M.; de Gouw, J. A. Laboratory Measurements of Trace Gas Emissions from Biomass Burning of Fuel Types from the Southeastern and Southwestern United States. *Atmos. Chem. Phys.* **2010**, *10* (22), 11115−11130.
(63) Cappa, C. D. A Model of Aerosol Evaporation Kinetics in a Thermodenuder. *Atmos. Meas. Technol.* **2010**, *3* (3), 579−592.
(64) Briggs, N. L.; Jaffe, D. A.; Gao, H.; Hee, J. R.; Baylon, P. M.; Zhang, Q.; Zhou, S.; Collier, S. C.; Sampson, P. D.; Cary, R. A. Particulate Matter, Ozone, and Nitrogen Species in Aged Wildfire Plumes Observed at the Mount Bachelor Observatory. *Aerosol Air Qual. Res.* **2016**, *16* (12), 3075−3087.
(65) Heald, C. L.; Kroll, J. H.; Jimenez, J. L.; Docherty, K. S.; Decarlo, P. F.; Aiken, A. C.; Chen, Q.; Martin, S. T.; Farmer, D. K.; Artaxo, P. A Simplified Description of the Evolution of Organic Aerosol Composition in the Atmosphere. *Geophys. Res. Lett.* **2010**, *37* (8), 1.
(66) Ng, N. L.; Canagaratna, M. R.; Jimenez, J. L.; Chhabra, P. S.; Seinfeld, J. H.; Worsnop, D. R. Changes in Organic Aerosol Composition with Aging Inferred from Aerosol Mass Spectra. *Atmos. Chem. Phys.* **2011**, *11* (13), 6465−6474.
(67) Gilardoni, S.; Massoli, P.; Paglione, M.; Giulianelli, L.; Carbone, C.; Rinaldi, M.; Decesari, S.; Sandrini, S.; Costabile, F.; Gobbi, G. P.; Pietrogrande, M. C.; Visentin, M.; Scotto, F.; Fuzzi, S.; Facchini, M. C. Direct Observation of Aqueous Secondary Organic Aerosol from Biomass-Burning Emissions. *Proc. Natl. Acad. Sci. U. S. A.* **2016**, *113* (36), 10013−10018.
(68) Yu, L.; Smith, J.; Laskin, A.; Anastasio, C.; Laskin, J.; Zhang, Q. Chemical Characterization of SOA Formed from Aqueous-Phase Reactions of Phenols with the Triplet Excited State of Carbonyl and Hydroxyl Radical. *Atmos. Chem. Phys.* **2014**, *14* (24), 13801−13816.
(69) Jiang, W.; Niedek, C.; Anastasio, C.; Zhang, Q. Photoaging of Phenolic Secondary Organic Aerosol in the Aqueous Phase: Evolution of Chemical and Optical Properties and Effects of Oxidants. *Atmos. Chem. Phys.* **2023**, *23* (12), 7103−7120.
(70) Yee, L. D.; Kautzman, K. E.; Loza, C. L.; Schilling, K. A.; Coggon, M.; Chhabra, P. S.; Chan, M. N.; Chan, A. W. H.; Hersey, S.;

Crounse, J. D.; Wennberg, P. O.; Flagan, R. C.; Seinfeld, J. H. Secondary Organic Aerosol Formation from Biomass Burning Intermediates: Phenol and Methoxyphenols. *Atmos. Chem. Phys.* **2013**, *13* (16), 8019−8043.
(71) Zhang, H.; Yang, B.; Wang, Y.; Shu, J.; Zhang, P.; Ma, P.; Li, Z. Gas-Phase Reactions of Methoxyphenols with NO3 Radicals: Kinetics, Products, and Mechanisms. *J. Phys. Chem. A* **2016**, *120* (8), 1213−1221.
(72) Schauer, J. J.; Kleeman, M. J.; Cass, G. R.; Simoneit, B. R. T. Measurement of Emissions from Air Pollution Sources. 3. C1-C29 Organic Compounds from Fireplace Combustion of Wood. *Environ. Sci. Technol.* **2001**, *35* (9), 1716−1728.
(73) Simpson, C. D.; Paulsen, M.; Dills, R. L.; Liu, L. S.; Kalman, D. A. Determination of Methoxyphenols in Ambient Atmospheric Particulate Matter: Tracers for Wood Combustion. *Environ. Sci. Technol.* **2005**, *39* (2), 631−637.
(74) Bonnefoy, A.; Chiron, S.; Botta, A. Environmental Nitration Processes Enhance the Mutagenic Potency of Aromatic Compounds. *Environ. Toxicol.* **2012**, *27*, 321.
(75) Adachi, K.; Sedlacek, A. J.; Kleinman, L.; Springston, S. R.; Wang, J.; Chand, D.; Hubbe, J. M.; Shilling, J. E.; Onasch, T. B.; Kinase, T.; Sakata, K.; Takahashi, Y.; Buseck, P. R. Spherical Tarball Particles Form through Rapid Chemical and Physical Changes of Organic Matter in Biomass-Burning Smoke. *Proc. Natl. Acad. Sci. U. S. A.* **2019**, *116* (39), 19336−19341.
(76) Sun, Y. L.; Zhang, Q.; Anastasio, C.; Sun, J. Insights into Secondary Organic Aerosol Formed via Aqueous-Phase Reactions of Phenolic Compounds Based on High Resolution Mass Spectrometry. *Atmos. Chem. Phys.* **2010**, *10* (10), 4809−4822.
(77) Li, C.; He, Q.; Schade, J.; Passig, J.; Zimmermann, R.; Meidan, D.; Laskin, A.; Rudich, Y. Dynamic Changes in Optical and Chemical Properties of Tar Ball Aerosols by Atmospheric Photochemical Aging. *Atmos. Chem. Phys.* **2019**, *19* (1), 139−163.
(78) *Mass Spctral Correlations*, 2nd ed.; McLafferty, F. W., Venkataraghavan, R., Eds.; American Chemical Society, 1982. DOI: 10.1021/ba-1982-0040.
(79) Day, D. A.; Campuzano-Jost, P.; Nault, B. A.; Palm, B. B.; Hu, W.; Guo, H.; Wooldridge, P. J.; Cohen, R. C.; Docherty, K. S.; Huffman, J. A.; De Sá, S. S.; Martin, S. T.; Jiménez, J. L. A Systematic Re-Evaluation of Methods for Quantification of Bulk Particle-Phase Organic Nitrates Using Real-Time Aerosol Mass Spectrometry. *Atmos. Meas. Technol.* **2022**, *15*, 459.
(80) Ge, D.; Nie, W.; Sun, P.; Liu, Y.; Wang, T.; Wang, J.; Wang, J.; Wang, L.; Zhu, C.; Wang, R.; Liu, T.; Chi, X.; Ding, A. Characterization of Particulate Organic Nitrates in the Yangtze River Delta, East China, Using the Time-of-Flight Aerosol Chemical Speciation Monitor. *Atmos. Environ.* **2022**, *272*, 118927.
(81) Li, J.; Pósfai, M.; Hobbs, P. V.; Buseck, P. R. Individual Aerosol Particles from Biomass Burning in Southern Africa: 2. Compositions and Aging of Inorganic Particles. *J. Geophys. Res. D Atmos.* **2003**, *108* (13), 1−12.
(82) Andreae, M. O. Soot Carbon and Excess Fine Potassium: Long-Range Transport of Combustion-Derived Aerosols. *Science (80-.).* **1983**, *220* (4602), 1148−1151.
(83) Chen, L.-W. A.; Moosmuller, H.; Arnott, W. P.; Chow, J. C.; Watson, J. G.; Susott, R. A.; Babbitt, R. E.; Wold, C. E.; Lincoln, E. N.; Hao, W. M. Emissions from Laboratory Combustion of Wildland Fuels: Emission Factors and Source Profiles. *Environ. Sci. Technol.* **2007**, *41* (12), 4317−4325.
(84) McMeeking, G. R.; Kreidenweis, S. M.; Baker, S.; Carrico, C. M.; Chow, J. C.; Collett, J. L.; Hao, W. M.; Holden, A. S.; Kirchstetter, T. W.; Malm, W. C.; Moosmuller, H.; Sullivan, A. P.; Wold, C. E. Emissions of Trace Gases and Aerosols during the Open Combustion of Biomass in the Laboratory. *J. Geophys. Res. Atmos.* **2009**, *114* (D19), 1.
(85) Pratt, K. A.; Murphy, S. M.; Subramanian, R.; Demott, P. J.; Kok, G. L.; Campos, T.; Rogers, D. C.; Prenni, A. J.; Heymsfield, A. J.; Seinfeld, J. H.; Prather, K. A. Flight-Based Chemical Characterization of Biomass Burning Aerosols within Two Prescribed Burn Smoke Plumes. *Atmos. Chem. Phys.* **2011**, *11* (24), 12549−12565.
(86) Pratt, K. A.; Heymsfield, A. J.; Twohy, C. H.; Murphy, S. M.; DeMott, P. J.; Hudson, J. G.; Subramanian, R.; Wang, Z.; Seinfeld, J. H.; Prather, K. A. In Situ Chemical Characterization of Aged Biomass-Burning Aerosols Impacting Cold Wave Clouds. *J. Atmos. Sci.* **2010**, *67* (8), 2451−2468.
(87) Zauscher, M. D.; Wang, Y.; Moore, M. J. K.; Gaston, C. J.; Prather, K. A. Air Quality Impact and Physicochemical Aging of Biomass Burning Aerosols during the 2007 San Diego Wildfires. *Environ. Sci. Technol.* **2013**, *47* (14), 7633−7643.
(88) Farley, R. N.; Collier, S.; Cappa, C. D.; Williams, L. R.; Onasch, T. B.; Russell, M.; Kim, H.; Zhang, Q. Source Apportionment of Soot Particles and Aqueous-Phase Processing of Black Carbon Coatings in an Urban Environment. *Atmos. Chem. Phys.* **2023**, *23* (23), 15039−15056.
(89) Drewnick, F.; Diesch, J. M.; Faber, P.; Borrmann, S. Aerosol Mass Spectrometry: Particle-Vaporizer Interactions and Their Consequences for the Measurements. *Atmos. Meas. Technol.* **2015**, *8* (9), 3811−3830.
(90) Sorvajärvi, T.; DeMartini, N.; Rossi, J.; Toivonen, J. In Situ Measurement Technique for Simultaneous Detection of K, KCl, and KOH Vapors Released during Combustion of Solid Biomass Fuel in a Single Particle Reactor. *Appl. Spectrosc.* **2014**, *68* (2), 179−184.
(91) Cao, W.; Martí-Rosselló, T.; Li, J.; Lue, L. Prediction of Potassium Compounds Released from Biomass during Combustion. *Appl. Energy* **2019**, *250* (May), 1696−1705.
(92) Li, B.; Sun, Z.; Li, Z.; Aldén, M.; Jakobsen, J. G.; Hansen, S.; Glarborg, P. Post-Flame Gas-Phase Sulfation of Potassium Chloride. *Combust. Flame* **2013**, *160* (5), 959−969.
(93) Wang, Y.; Hu, M.; Xu, N.; Qin, Y.; Wu, Z.; Zeng, L.; Huang, X.; He, L. Chemical Composition and Light Absorption of Carbonaceous Aerosols Emitted from Crop Residue Burning: Influence of Combustion Efficiency. *Atmos. Chem. Phys.* **2020**, *20* (22), 13721−13734.
(94) McClure, C. D.; Lim, C. Y.; Hagan, D. H.; Kroll, J. H.; Cappa, C. D. Biomass-Burning-Derived Particles from a Wide Variety of Fuels - Part 1: Properties of Primary Particles. *Atmos. Chem. Phys.* **2020**, *20* (3), 1531−1547.
(95) Dzepina, K.; Arey, J.; Marr, L.; Worsnop, D. R.; Salcedo, D.; Zhang, Q.; Onasch, T. B.; Molina, L.; Molina, M. J.; Jimenez, J. L. Detection of Particle-Phase Polycyclic Aromatic Hydrocarbons in Mexico City Using an Aerosol Mass Spectrometer. *Int. J. Mass Spectrom.* **2007**, *263* (2), 152−170.
(96) Zheng, G.; Sedlacek, A. J.; Aiken, A. C.; Feng, Y.; Watson, T. B.; Raveh-Rubin, S.; Uin, J.; Lewis, E. R.; Wang, J. Long-Range Transported North American Wildfire Aerosols Observed in Marine Boundary Layer of Eastern North Atlantic. *Environ. Int.* **2020**, *139*, 105680.
(97) Engelmann, R.; Ansmann, A.; Ohneiser, K.; Griesche, H.; Radenz, M.; Hofer, J.; Althausen, D.; Dahlke, S.; Maturilli, M.; Veselovskii, I.; Jimenez, C.; Wiesen, R.; Baars, H.; Bühl, J.; Gebauer, H.; Haarig, M.; Seifert, P.; Wandinger, U.; Macke, A. Wildfire Smoke, Arctic Haze, and Aerosol Effects on Mixed-Phase and Cirrus Clouds over the North Pole Region during MOSAiC: An Introduction. *Atmos. Chem. Phys.* **2021**, *21*, 13397−13423.
(98) Kommula, S. M.; Buchholz, A.; Gramlich, Y.; Mielonen, T.; Hao, L.; Pullinen, I.; Vettikkat, L.; Ylisirniö, A.; Joutsensaari, J.; Schobesberger, S.; Tiitta, P.; Leskinen, A.; Hesslin-Rees, D.; Haslett, S. L.; Siegel, K.; Lunder, C.; Zieger, P.; Krejci, R.; Romakkaniemi, S.; Mohr, C.; Virtanen, A. Effect of Long - Range Transported Fire Aerosols on Cloud Condensation Nuclei Concentrations and Cloud Properties at High Latitudes. *Geophys. Res. Lett.* **2024**, *51*, e2023GL107134.
(99) Lee, J. E.; Gorkowski, K.; Meyer, A. G.; Benedict, K. B.; Aiken, A. C.; Dubey, M. K. Wildfire Smoke Demonstrates Significant and Predictable Black Carbon Light Absorption Enhancements. *Geophys. Res. Lett.* **2022**, *49* (14), 49.